

MEASURING ROTATION PERIODS IN CROWDED STAR CLUSTERS WITH TESS: A PROOF-OF-CONCEPT WITH NGC 3532

MATTHEW S. STAFFORD ¹, JASON LEE CURTIS ¹ AND MARCEL A. AGÜEROS ^{1,2}

¹*Department of Astronomy, Columbia University, 550 West 120th Street, New York, NY 10027, USA*

²*Laboratoire d'astrophysique de Bordeaux, Université de Bordeaux, CNRS, B18N, Allée Geoffroy Saint-Hilaire, 33615 Pessac, France*

(Accepted January 20, 2026)

ABSTRACT

The Transiting Exoplanet Survey Satellite (TESS) has observed nearly the entire sky, producing full-frame images (FFIs) every 30 min (Cycles 1–2), 10 min (Cycles 3–4), and now 200 s (Cycle 5+), over 27-day sectors. Light curves extracted from FFIs can be used to measure stellar rotation periods (P_{rot}) in nearby open clusters, and are well-suited for studying low-mass stars ($\lesssim 1.2 M_{\odot}$) younger than $\lesssim 1$ Gyr, whose P_{rot} are generally still ≤ 15 days. A challenge to exploiting TESS data fully is its $21''$ pixel size, which can cause strong signals from a source to contaminate the signals of nearby sources in the crowded environments found, e.g., in the more distant and/or richest clusters. We conducted a test with the young (≈ 350 Myr old), moderately distant (470 pc), and rich open cluster NGC 3532 ($N_{\star} > 3000$), which has an extensive P_{rot} catalog from ground-based photometry, to examine the reliability of P_{rot} obtained from TESS data. We recovered 69% of the literature periods from at least one of the three TESS cycles in which NGC 3532 was observed before any quality analysis. We then used all available TESS data for low-mass members of NGC 3532 and, applying a set of quality cuts that combined information from TESS and from Gaia, measured P_{rot} for 885 cluster stars, adding 706 new P_{rot} to the existing catalog. We conclude that, when considered with appropriate caution, TESS data for stars in crowded fields can yield reliable P_{rot} measurements.

Keywords: Low mass stars (2050) — Open star clusters (1160) — Stellar rotation (1629)

1. INTRODUCTION

Unlike its predecessor Kepler (and then K2; [W. J. Borucki et al. 2010](#), [S. B. Howell et al. 2014](#)), NASA's Transiting Exoplanet Survey Satellite (TESS; [G. R. Ricker et al. 2015](#)) is a (nearly) all-sky telescope. TESS data can therefore be used to measure the P_{rot} of cool main-sequence stars across much of the sky (e.g., [J. L. Curtis et al. 2019](#), [F. Anthony et al. 2022](#), [E. R. Newton et al. 2022](#), [E. K. Pass et al. 2022](#), [L. M. Rebull et al. 2022](#), [A. Frasca et al. 2023](#), [M. Popinchalk et al. 2023](#), [R. P. Petrucci et al. 2024](#), [Z. R. Clayton et al. 2024](#), [I. L. Colman et al. 2024](#)). However, TESS's pixels are large ($21''$ vs. $4''$ for Kepler/K2), potentially limiting the usefulness of these data for measuring P_{rot} in distant clus-

ters and/or crowded Galactic fields due to photometric contamination from nearby stars (see Figure 1).

We used the open cluster NGC 3532 (R.A. = $11^{\text{h}}06^{\text{m}}$, decl. = $-58^{\circ}42'$, J2000) as a test case for determining the robustness of P_{rot} measurements made from light curves extracted from TESS FFIs in crowded fields. NGC 3532, observed during TESS Cycles 1, 3, and 5 at the time of this study, is ≈ 350 Myr old, relatively distant (470 pc) and rich, with several thousand members ([J. D. Cummings & J. S. Kalirai 2018](#), [T. Cantat-Gaudin et al. 2018](#), [D. J. Fritzewski et al. 2019](#), [M. Kounkel & K. Covey 2019](#), [E. L. Hunt & S. Reffert 2023](#)). Furthermore, the cluster is centrally concentrated and located in the Galactic plane. This makes it an excellent test case for studying the impact on period measurements of other variable cluster members or of the large numbers of variable stars in the Galactic background that may contaminate our TESS light curves. NGC 3532 also has a recent and extensive P_{rot} catalog derived from ground-

Corresponding author: Matthew S. Stafford
 ms5750@columbia.edu

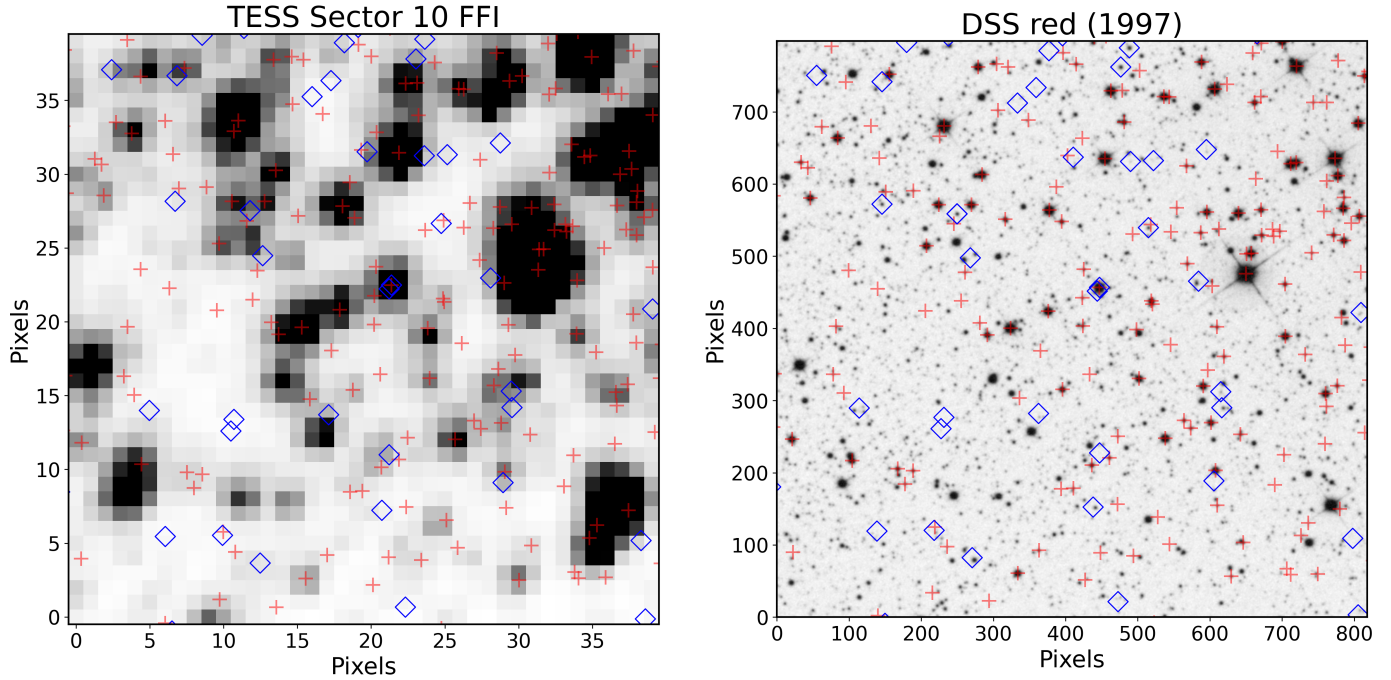


Figure 1. Comparison of a TESS Sector 10 FFI 40×40 pixel cutout (left) and ground-based DSS image (right) for a representative cluster target. The red plus symbols are the 159 E. L. Hunt & S. Reffert (2023) cluster members in the image, and the blue diamonds are 32 variables included in the Gaia DR3 variability catalog (L. Eyer et al. 2023). Clearly, the TESS pixels are large enough to include contributions from several sources, including background variables.

based observations (D. J. Fritzewski et al. 2021a) with which to compare our TESS-based measurements.

Using TESS full-frame images (FFIs), we constructed light curves for 1358 members of NGC 3532 based on the E. L. Hunt & S. Reffert (2023) catalog, and generated periodograms to find the most likely TESS-based P_{rot} for each observation of these stars. We first tested the usefulness of this automated approach by focusing on the subset of the 1358 members that are in the D. J. Fritzewski et al. (2021a) catalog, and found that we recovered a P_{rot} within 15% of these authors' value for 182/264 (69%) stars in at least one TESS cycle. Such a high recovery rate, without any post-processing to verify the quality of the P_{rot} measurements, indicated that these TESS data can be used to successfully measure P_{rot} in this relatively crowded field.

We therefore undertook a comprehensive analysis of the quality of our measurements to produce an expanded P_{rot} catalog for the cluster. By applying various quality constraints to our automatic measurements to remove those we determined to be of low quality, and by examining the impact of e.g., source confusion, we obtained confident P_{rot} measurements for 885 members of NGC 3532, 179 of which have a D. J. Fritzewski et al. (2021a) P_{rot} measurement, and 706 of which did not previously have a reported P_{rot} .

Our approach differs from the standard point-spread-function and difference-imaging techniques used to deblend TESS data and produce light curves for studying, e.g., transiting exoplanets and eclipsing binaries (e.g., R. J. Oelkers & K. G. Stassun 2018, L. G. Bouma et al. 2019, A. D. Feinstein et al. 2019, T. Han & T. D. Brandt 2023, D. Nardiello et al. 2019). These typically assume a constant flux for sources neighboring a target, making blending from variable sources a persistent concern.

Our approach also differs from other approaches that address the effects of blending by identifying variable sources that are contaminating the targets' signals. For example, with the package `TESS_localize` (M. E. Higgins & K. J. Bell 2023), one can use a frequency-based analysis to localize the source(s) of the variability measured in a given light curve. We focused instead on identifying the likely contaminating sources of the measured variability based on for example, constructing periodograms across multiple pixels, as was done for Kepler data by I. L. Colman et al. (2017).

We then repeated our comparison with the P_{rot} from D. J. Fritzewski et al. (2021a) catalog, now using final P_{rot} from our expanded catalog. The overall agreement between the two sets of measurements is 77%, and it is as high as 86% for the D. J. Fritzewski et al. (2021a) class 1 P_{rot} , which are these authors' most confident measurements. We concluded that our approach, which

relies only on data from TESS and from Gaia, can be fruitfully applied to other (relatively) crowded stellar fields, and in particular to clusters that do not have an existing P_{rot} catalog.

This paper is structured as follows: in Section 2, we discuss the D. J. Fritzewski et al. (2019; 2021a,b) studies of NGC 3532, which provided us with the comparison sample of P_{rot} with which we tested our TESS-based P_{rot} measurements. We also describe the E. L. Hunt & S. Reffert (2023) NGC 3532 cluster membership catalog, which we used to expand the rotation catalog for the cluster. In Section 3, we discuss our procedure for measuring P_{rot} from light curves extracted from TESS FFIs, and describe quality filters applied to these measurements to improve the reliability of the P_{rot} samples obtained. In Section 4, we provide the updated P_{rot} catalog for NGC 3532 that incorporates the application of our P_{rot} measurement technique to the TESS data, and compare our final P_{rot} measurements to those of D. J. Fritzewski et al. (2021a). We conclude in Section 5.

2. THE EXISTING ROTATION AND MEMBERSHIP CATALOGS FOR NGC 3532

2.1. The D. J. Fritzewski et al. Studies of the Cluster

In the first in a series of three papers, D. J. Fritzewski et al. (2019) produced a membership catalog for NGC 3532, supplementing Gaia Data Release 2 (DR2; Gaia Collaboration et al. 2018) proper motions with radial velocity measurements from the literature and from their own observations, and identifying 660 high-confidence members.

D. J. Fritzewski et al. (2021a) then imaged NGC 3532 in the V and I_c bands over the course of ≈ 40 consecutive nights with the Yale 1-m telescope at the Cerro Tololo Inter-American Observatory, Chile. D. J. Fritzewski et al. (2021a) used these data to identify 165 rotators among the radial velocity cluster members, and an additional 11 rotators among Gaia DR2 proper motion members for which D. J. Fritzewski et al. (2019) did not obtain radial velocities.

Finally, D. J. Fritzewski et al. (2021b) used spectra of the Ca II infrared triplet (IRT) obtained with the AAOmega spectrograph on the 3.9-m Anglo-Australian Telescope, Australia, to measure chromospheric emission ratios R'_{IRT} for 454 cluster members. These authors derived an empirical rotation–activity relationship with these measurements and P_{rot} from D. J. Fritzewski et al. (2021a), and then predicted P_{rot} based on R'_{IRT} measurements for stars for which D. J. Fritzewski et al. (2021a) had not measured photometric P_{rot} . D. J. Fritzewski et al. (2021b) used the predicted periods as priors when searching those stars’ light curves for P_{rot} ,

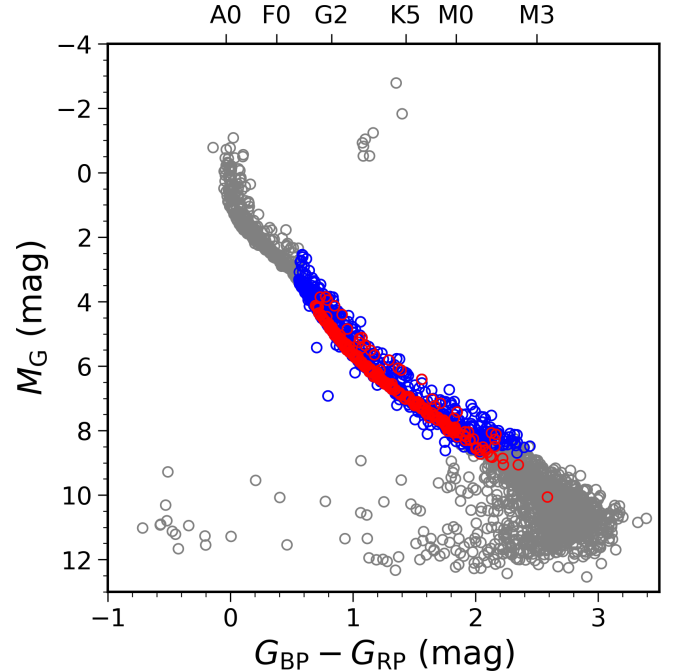


Figure 2. Gaia CMD for NGC 3532 based on the E. L. Hunt & S. Reffert (2023) catalog of 3414 members. The absolute magnitudes were calculated using inverted Gaia DR3 parallaxes; we applied a reddening $A_V = 0.093$ mag (J. D. Cummings & J. S. Kalirai 2018). The red circles are the 276 stars in the E. L. Hunt & S. Reffert (2023) catalog with D. J. Fritzewski et al. (2021a) P_{rot} measurements. The blue circles are the 1358 low-mass, main-sequence cluster members for which we have TESS light curves and that met our selection criteria for making new P_{rot} measurements.

and in this manner reported P_{rot} for 103 additional NGC 3532 members.³

These D. J. Fritzewski et al. (2021b) P_{rot} were included in the D. J. Fritzewski et al. (2021a) sample. This sample therefore includes 279 P_{rot} for F, G, K, and M members of NGC 3532, divided into four classes that reflect their quality and how they were derived. Class 1 P_{rot} are measured from light curves with signals clearly evident with visual inspection (93 P_{rot}), class 2 are photometrically derived from light curves with less clear signals (66 P_{rot}), and class 3 are activity-informed (103 P_{rot}); in addition, periods that are possible aliases were labeled class 0 (17 P_{rot}).

The majority of these rotators fall on the sequence of (relatively) slowly rotating stars in the color–period diagram (CPD) for the cluster, extending from ≈ 4 days

³While the D. J. Fritzewski et al. (2021a,b) papers stated that P_{rot} for 113 additional stars were obtained using activity measurements in this manner, the published catalog only includes 103 such stars.

for the late F stars to ≈ 15 days for the late K/early M stars (see figure 6 in [D. J. Fritzewski et al. 2021a](#)). This is consistent with expectations from younger and older clusters that show these slow-rotating sequences across this same mass range (e.g., at ≈ 120 Myr in the Pleiades, and at ≈ 700 Myr in the Hyades, Praesepe, and Coma Berenices; [S. A. Barnes 2003; 2007](#), [K. R. Covey et al. 2016](#), [L. M. Rebull et al. 2016](#), [S. T. Douglas et al. 2019](#), [R. Rampalli et al. 2021](#), [M. A. Agüeros et al. 2025](#)).

2.2. The [E. L. Hunt & S. Reffert \(2023\)](#) Membership Catalog

Even in the case of historical clusters such as NGC 3532, known by Western astronomers since the 18th century and greatly appreciated by no less a figure than John Herschel,⁴ Gaia data have proved extremely useful in improving studies of membership. By applying the HDBSCAN algorithm ([R. J. G. B. Campello et al. 2013](#), [L. McInnes et al. 2017](#)) to the Gaia Data Release 3 (DR3; [Gaia Collaboration et al. 2023](#)), [E. L. Hunt & S. Reffert \(2023\)](#) found that NGC 3532 has 3414 members.^{5,6} The [E. L. Hunt & S. Reffert \(2023\)](#) catalog is shown in the color–magnitude diagram (CMD) in Figure 2.

The [E. L. Hunt & S. Reffert \(2023\)](#) membership catalog for NGC 3532 includes 627 of the 660 high-confidence members from [D. J. Fritzewski et al. \(2019\)](#). The overlap between catalogs is even greater for the rotators identified by Fritzewski et al. Of the 279 stars in the [D. J. Fritzewski et al. \(2021a\)](#) P_{rot} catalog, 276 are included in the [E. L. Hunt & S. Reffert \(2023\)](#) membership catalog; we highlight these stars in Figure 2, and adopt the [E. L. Hunt & S. Reffert \(2023\)](#) catalog for this study.

3. MEASURING P_{rot} FOR NGC 3532 MEMBERS

3.1. Assembling and Analyzing TESS Light Curves for 1358 Cluster Stars

We restricted our search for TESS data to the [E. L. Hunt & S. Reffert \(2023\)](#) stars that met the following criteria: $(G_{\text{BP}} - G_{\text{RP}}) > 0.6$ mag, to remove stars lacking a convective outer envelope; $G > 9$ mag, to remove giants; and $G < 17$, to limit our analysis to stars bright enough

⁴Herschel described NGC 3532 as “a glorious cluster of immense magnitude” in his observing logs from his time in South Africa (1834–1838). The only other objects for which he used the adjective glorious are ω Cen and 47 Tuc ([S. Herschel 1847](#)).

⁵HDBSCAN, which is based on DBSCAN, finds clusters based on the density of data points. [E. L. Hunt & S. Reffert \(2021\)](#) tested various clustering algorithms and argued that the most effective method for identifying cluster members in Gaia data is to use HDBSCAN with some post-processing to remove contaminants.

⁶Gaia DR3 improved on DR2 parallax precisions by 30% and proper motion precisions by $\times 2$ ([Gaia Collaboration et al. 2023](#)).

Table 1. TESS observations of NGC 3532

	Cadence	Sectors	Date	# of Stars ^a
Cycle 1	30 min	10, 11	2019 March 26–May 20	1357
Cycle 3	10 min	36, 37	2021 March 7–April 28	1054
Cycle 5	200 s	63, 64	2023 March 10–May 4	1341

^aThe numbers quoted here are for the low-mass stars that met our selection criteria. In total, 1036 such stars were observed in all three cycles, while 322 were observed in two of the three cycles.

that their TESS light curves are usable. The overlap between the [E. L. Hunt & S. Reffert \(2023\)](#) and [D. J. Fritzewski et al. \(2021a\)](#) catalog described in Section 2.2 (276 stars) includes 12 stars with $G > 17$ mag that did not meet our criteria for P_{rot} measurement. This left us with 264 stars for which we could compare our P_{rot} measurements to that from [D. J. Fritzewski et al. \(2021a\)](#).

Of the 1358 stars in the complete [E. L. Hunt & S. Reffert \(2023\)](#) catalog that met these criteria, 1036 were observed in Cycles 1, 3, and 5, while the remaining 322 were observed in two of the three cycles (see Table 1; these 1358 stars are highlighted in Figure 2). Of these stars, 391 have a $G < 17$ mag cluster member within 1', and 789 have one within 2', underscoring the potential for source confusion in this sample.

We first downloaded 40×40 pixel FFI cutouts ([STScI 2022](#)) with TESScut ([C. E. Brasseur et al. 2019](#)) for our 1358 targets. We then used Causal Pixel Modeling (CPM; [D. Wang et al. 2016](#)), as implemented in the Python package `unpopular` ([S. Hattori et al. 2022](#)), to produce light curves. `unpopular` models and subtracts time-varying systematics based on the behavior of pixels outside an exclusion region centered on the target (the central 9×9 pixels in our case).

The increasing observing cadence between Cycles 1, 3, and 5 raises the photometric noise, which can suppress the periodogram power for otherwise equivalent signals. For this reason and to limit data volume, we binned all the light curves down to 30 min.

When stars were observed in consecutive sectors (common in Cycles 1 and 5), we joined the light curves, thereby extending the temporal coverage from 27 to 54 days, and treated them as a single light curve. While these longer-baseline light curves open the possibility of measuring longer P_{rot} , we did not expect a significant number of NGC 3532 stars to have $P_{\text{rot}} > 15$ days because of the cluster’s relatively young age. Of the 279 stars with a measured P_{rot} in the [D. J. Fritzewski et al. \(2021a\)](#) catalog, only 11 (4%) have $P_{\text{rot}} > 15$ days. Moreover, none of these were categorized as class 1 pe-

riods by D. J. Fritzewski et al. (2021a): one is classified as class 2, and the remaining 10 are class 3 (i.e., activity-informed), indicating that these are not among the highest-confidence P_{rot} measured by these authors.⁷

Furthermore, using light curves produced by stitching together data from multiple TESS sectors to measure longer P_{rot} for a star is challenging (e.g., F. Anthony et al. 2022). New approaches may eventually allow us to extend our investigation to longer P_{rot} (e.g., Z. R. Claytor et al. 2024, S. Hattori et al. 2025), but for this study we discounted any >15 days P_{rot} we measured.

We used `astropy.timeseries` to calculate Lomb–Scargle (LS) periodograms (N. R. Lomb 1976, J. D. Scargle 1982, W. H. Press & G. B. Rybicki 1989) with test periods spaced logarithmically between 0.1 and 30 days. As discussed in Section 3.4, we produced both one- and two-term LS periodograms, with the latter used to search for and correct harmonic P_{rot} measurements (as done by I. L. Colman et al. 2024). We recorded the period and power for the top two peaks in our periodograms for each available cycle for the 1358 NGC 3532 stars we considered. For 182/264 (69%) stars in the D. J. Fritzewski et al. (2021a) catalog for which we recorded periods at this step, the period associated with the primary periodogram peak for at least one TESS cycle agreed with the P_{rot} from D. J. Fritzewski et al. (2021a) within 15%. Following this initial comparison, we analyzed our measured P_{rot} to develop a method to identify which of our measurements were robust and to remove those that were spurious.

In the left column of Figure 3, we show CPDs for the three TESS cycles using the automatically measured TESS P_{rot} and Gaia ($G_{\text{BP}} - G_{\text{RP}}$) colors. In each CPD, there is, as expected, a densely populated sequence of slowly rotating stars, the position of which is related to the cluster’s age. Also visible are clearly erroneous measurements due to e.g., noise, half-period harmonics, and systematic errors, such as the population of 3 day rotators in the top left panel, for Cycle 1. Still, the presence of a well-defined period sequence in the CPDs for all three cycles before *any* assessment of measurement quality demonstrates the potential to retrieve accurate P_{rot} measurements.

To identify cases where the TESS-derived P_{rot} are inaccurate, we examined the FFIs, light curves extracted

⁷Although we did not expect to recover accurate P_{rot} for these 11 stars, we included them in our later comparison of our results and those of D. J. Fritzewski et al. (2021a) to assess the effectiveness of our method in removing inaccurate or unreliable P_{rot} for slow rotators.

from the pixel hosting a given target and from pixels in surrounding annuli, the associated periodograms, and characteristics of neighboring targets (e.g., G magnitude, separation on the sky, P_{rot}). In the remainder of this section, we will describe the several ways we removed spurious measurements from our sample.

3.2. Removing P_{rot} Measurements That Result From Systematics or That Are Marginal Detections

Our first step was to set a periodogram power threshold for the P_{rot} measurements from each TESS cycle, thereby removing weak signals or otherwise low-quality P_{rot} measurements from our sample. A 30th percentile threshold was applied to all measurements for a given cycle, corresponding to powers of ≈ 0.05 , ≈ 0.04 , and ≈ 0.03 , for Cycles 1, 3, and 5, respectively. This threshold was chosen to identify and remove the peak of low power measurements in the periodogram power histogram for each cycle (see the left panel of Figure 4, for Cycle 1 measurements). The right panel of Figure 4 shows the CPD with the low-power P_{rot} highlighted. This power threshold identified stars across the full range of ($G_{\text{BP}} - G_{\text{RP}}$) and P_{rot} , but especially later type stars that tend to be fainter and include some of the slowest rotators in our sample. Applying this minimum power requirement, we identified 377, 308, and 395 P_{rot} measurements for removal in the three cycles.

The CPDs in the left column of Figure 3 suggested that there are P_{rot} measurements that are the result of artificial signals in the TESS data. This is most evident in the top left panel, the CPD for Cycle 1, where there are a large number of P_{rot} between 3.0 and 3.5 days across the full range of color in our sample. Only some of these P_{rot} measurements are removed when applying the power requirement described above. The cause of this systematic error is not clear and affects stars distributed across the entire cluster. The periodograms produced from the affected light curves, however, all share a narrow primary peak at similar frequencies. We were able to identify the affected stars by selecting those P_{rot} measurements from Cycle 1 between 3.0 and 3.5 days with periodogram powers of < 0.1 . In this manner, we removed 68 P_{rot} that were not identified by the previously applied minimum power cut (see Figure 5).

There is another example of this kind of contamination in the Cycle 3 CPD. In the middle-left panel of Figure 3, there is an unexpected clump of P_{rot} measurements from 5 to 7 days for stars with $(G_{\text{BP}} - G_{\text{RP}}) < 0.75$ mag. We removed these erroneous P_{rot} measurements in the same fashion, by selecting P_{rot} measurements from Cycle 3 between 5.0 and 7.0 days with periodogram powers of < 0.1 , this time also constraining by ($G_{\text{BP}} - G_{\text{RP}}$). With

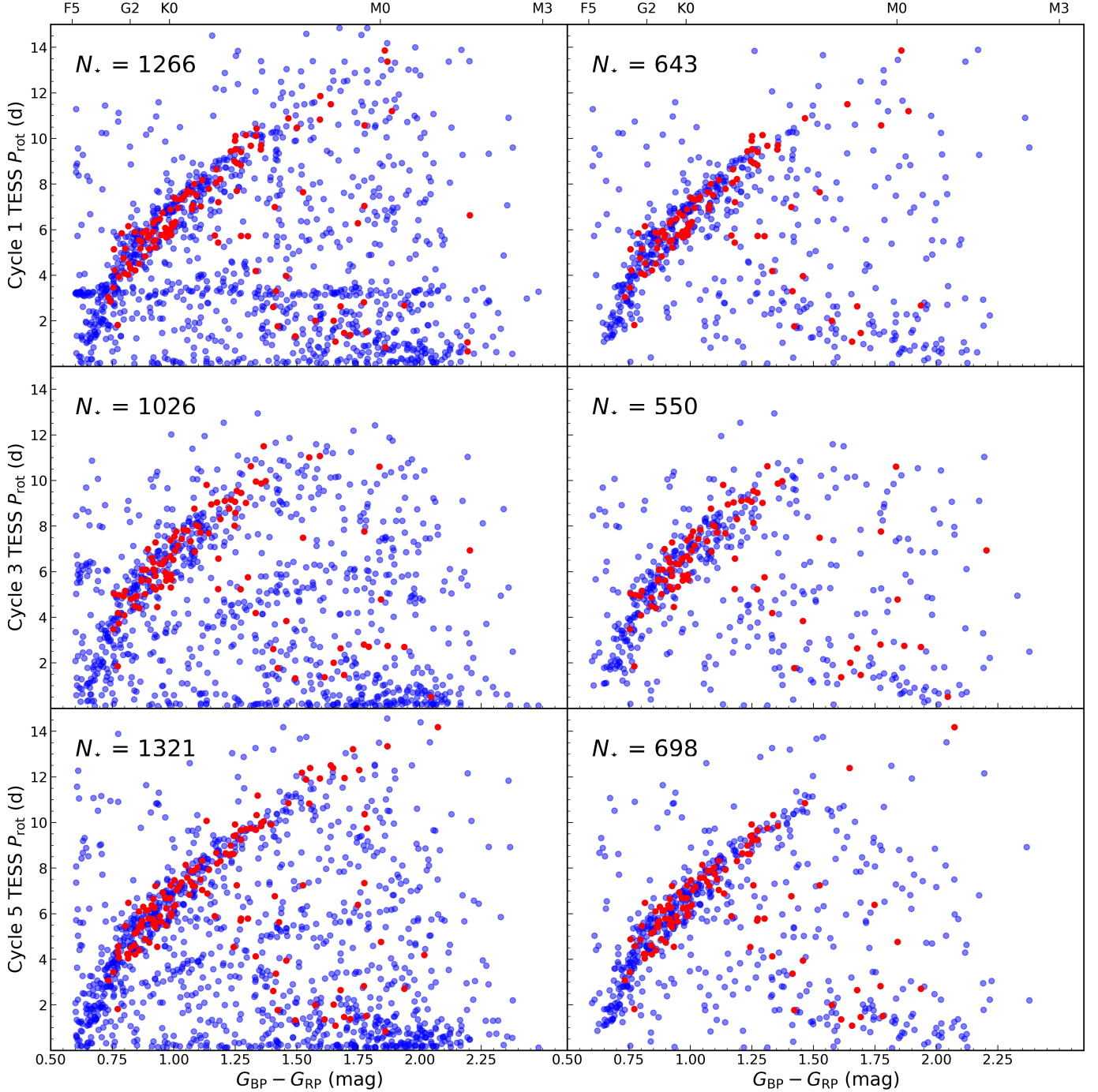


Figure 3. CPDs for NGC 3532 low-mass members with TESS light curves for each TESS cycle in which they were observed before (left) and after (right) our analysis removing erroneous measurements. As in Figure 2, blue circles represent our targets for P_{rot} measurement with TESS; red circles represent stars with a P_{rot} measurement that agrees with that from D. J. Fritzewski et al. (2021a) within 15%. In each CPD, we omit stars for which we measured $P_{\text{rot}} > 15$ days.

these criteria, we identified an additional 10 Cycle 3 P_{rot} measurements for removal from our sample.

Having access to multiple cycles of TESS data for the same stars also allowed us to identify likely unreliable short P_{rot} measurements. We identified the stars for which we measured a $P_{\text{rot}} < 1$ day that had a P_{rot}

from another cycle that was slower by at least 20%. The relatively easy detectability of rapid periodic signals makes it unlikely that a reliable <1 day P_{rot} measurement would disappear between TESS cycles. We identified 15, 15, and 31 of these rapid P_{rot} for removal in our samples for Cycles 1, 3, and 5, respectively.

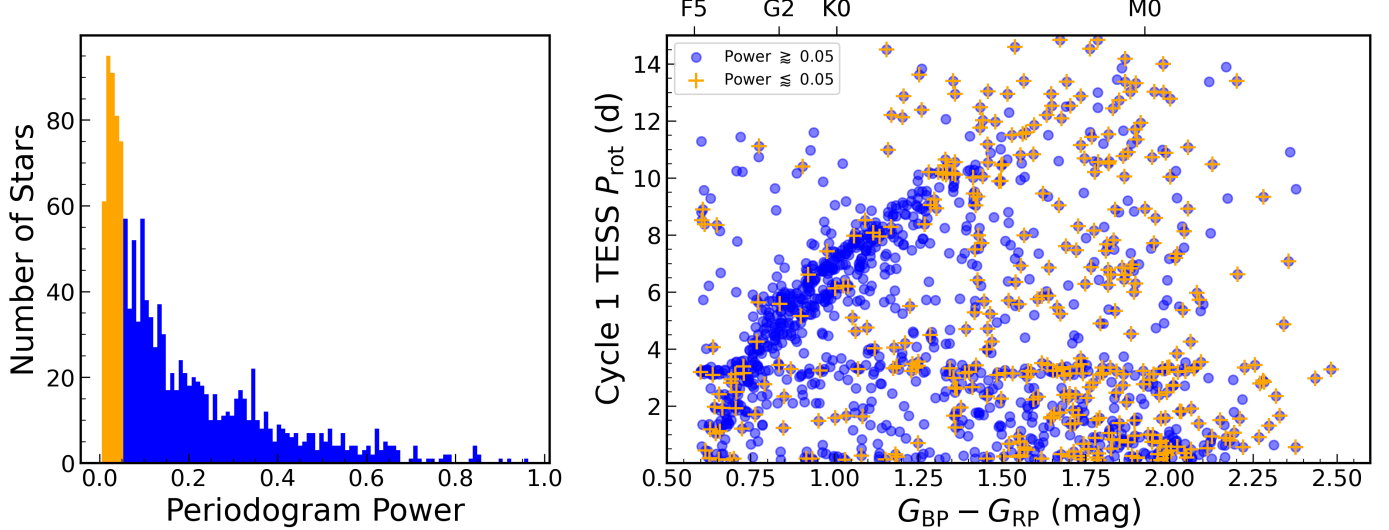


Figure 4. The impact on the Cycle 1 P_{rot} distribution of requiring a minimum power when validating P_{rot} measurements. The left panel is a histogram of the periodogram powers for the Cycle 1 light curves; the orange bins correspond to powers below the 30th percentile for this dataset (0.05 in this case). The right panel is the full distribution of Cycle 1 P_{rot} , with the values drawn from measurements with a power below the 30th percentile indicated with orange crosses. Those low-power measurements include many outliers, such as the K stars with $P_{\text{rot}} > 10$ days or <1 day, and other problematic measurements, such as the strip of ≈ 3 day P_{rot} across the observed color range.

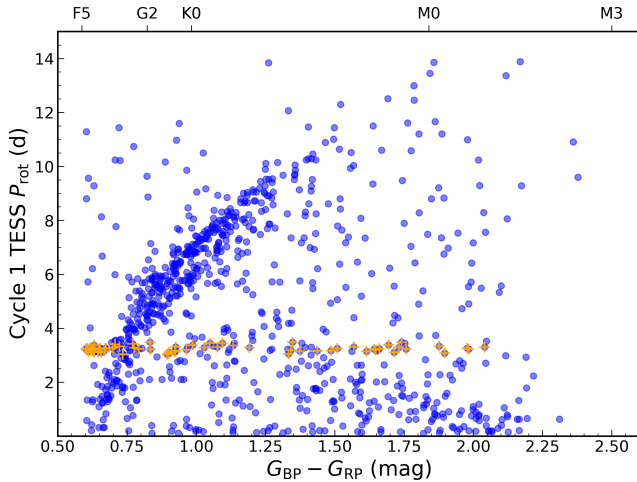


Figure 5. TESS Cycle 1 CPD depicting our identification of P_{rot} measurements that are the result of systematic errors. Measurements of $P_{\text{rot}} < 15$ days with periodograms powers greater than the 30th percentile power for this cycle are plotted as blue circles. P_{rot} measurements ranging from 3.0 to 3.5 days with periodogram powers <0.1 are marked with orange crosses and are likely the result of an (unspecified) systematic error in the Cycle 1 data. Setting a P_{rot} range and raising the minimum power required for consideration allows us to remove a number of unreliable measurements missed with the cut illustrated in Figure 4.

3.3. Identifying Cases of Source Confusion

The potential blending of signals from neighboring sources can be a source of inaccurate P_{rot} measurements when using TESS data for crowded fields. Since NGC 3532 is a young and rich cluster, we expected to detect many variable members, some of which may be near enough to other members to contaminate their light curves. The cluster’s location also raises the possibility that the Galactic background may provide many variable stars that can contaminate the TESS light curves.

In cases of source confusion, improperly assigned period measurements will often have high periodogram powers and appear to be robust. These measurements can therefore only be identified as erroneous using an analysis of nearby sources. We performed this analysis using two catalogs: our period measurements for NGC 3532, and the Gaia DR3 variability catalog (GVC; L. Eyer et al. 2023), which includes classifications based on 34 months of Gaia data for nearly 10^7 stars.

To illustrate the magnitude of the problem caused by variables in the Galactic background, we searched the GVC for stars within 90° of the center of NGC 3532, an area that contains 95% of the cluster’s membership. We found 4697 entries: 12 Cepheids (V. Ripepi et al. 2023), 195 RR Lyrae (G. Clementini et al. 2023), 3965 eclipsing binaries (EBs; N. Mowlavi et al. 2023), and 525 sources showing short-term variability on timescales $\lesssim 1$ day (M. Roelens et al. 2018).

3.3.1. An Example of Contamination by a Background Variable

A striking example of the impact of contamination by a background GVC source is the set of ≈ 2.1 day periods we measured in Cycle 1 for five cluster members ranging from $G = 12.4 - 14.4$ mag and within about $1'$ of each other on the sky (see Figure 6 for an FFI cutout of the field). Four of these five stars have P_{rot} measured by D. J. Fritzewski et al. (2021a), and these literature measurements are 2–4 times the length of the period we measured, which further raised our suspicions.

For each of the pixels shown in Figure 6, we produced a phase-folded light curve (see Figure 7) and a periodogram (see Figure 8). Examining the FFI and the corresponding light curves and periodograms, it became apparent that the likely source of the periodic signal measured for these cluster members is Gaia DR3 5340164256296564736, which is significantly brighter than our targets, with $G \approx 10.1$ mag. The GVC lists this star as a classical Cepheid, with a period of 2.1047 days and a G amplitude of 0.13 mag; the periodic signal we measure is caused by pulsations.⁸ Due to the star’s relative brightness and the rapid periodicity of its variability, its period is recoverable in light curves extracted from pixels several pixels removed from the star’s position, corresponding to a separation on the sky $>1'$.

This example illustrates how bright and rapidly variable sources can impact P_{rot} measurements for nearby stars.

3.3.2. Mitigating Source Confusion

For each TESS observation of our 1358 cluster targets, we checked the GVC for sources within $2'$ with periods (or harmonics/subharmonics) within 10% of the P_{rot} we measured. This resulted in the removal of 94, 85, and 115 P_{rot} that were not removed in previous steps from our samples for Cycles 1, 3, and 5, respectively. Unsurprisingly, given their relative frequency in the GVC, nearly all of the measurements we removed had periods matching that of a nearby EB.

We performed a similar search for possible contamination due to other NGC 3532 members. We first expanded the sample of members we considered as potential contaminants by constructing light curves for 389 stars in the E. L. Hunt & S. Reffert (2023) membership catalog that did not meet our initial criteria for P_{rot} .

⁸Although older studies included this star, designated as “NGC 3532 147” in SIMBAD, as a member of NGC 3532 (D. Koelbloed 1959, J. A. Fernandez & C. W. Salgado 1980), Gaia DR3 5340164256296564736 has been omitted from the recent Gaia-based catalogs (M. Kounkel et al. 2020, E. L. Hunt & S. Reffert 2023) as it is at a distance of 2.2 kpc.

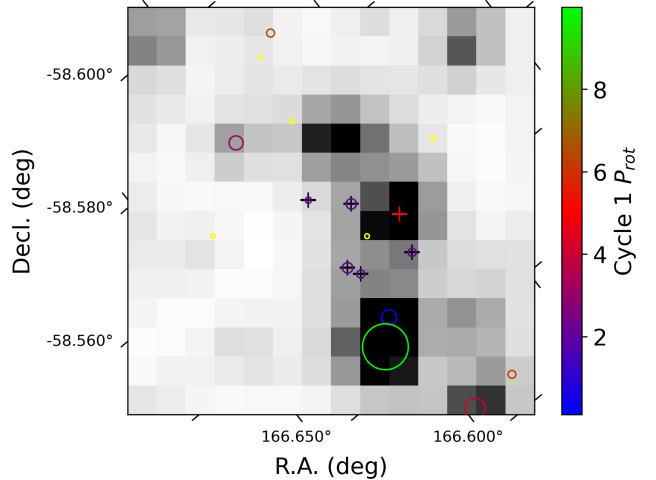


Figure 6. 14×14 pixel FFI cutout showing the Cycle 1 field containing the Cepheid Gaia DR3 5340164256296564736, indicated by the red cross. The circles are NGC 3532 members; the size of the circle is related to the star’s G magnitude, with larger circles being brighter. The colors of the circles are based on the P_{rot} we measured: yellow circles are cluster members for which we do not measure any P_{rot} because they are too faint, while the black crosses are members for which we measured a 2.1 day P_{rot} that is inaccurate and caused by contamination from the Cepheid. This example demonstrates how bright and rapidly varying sources can prevent accurate P_{rot} measurement for nearby targets when using TESS data.

measurement, but whose TESS data are usable (i.e., stars with $(G_{\text{BP}} - G_{\text{RP}}) < 0.6$ mag or $G < 9$), and measured their variability.⁹ We then had a sample of 1747 stars to use for this search.

For each TESS observation of our 1358 targets, we then checked whether any of the other 1746 members were within $2'$ on the sky and had a variability measurement within 1% of our target’s P_{rot} . We removed any such P_{rot} from our sample if the corresponding periodogram power was less than or equal to the power of the measurement associated with the potential contaminating signal.

In addition, for stars with P_{rot} measured in multiple cycles, we checked the agreement between the P_{rot} measurements across the cycles. If in a given cycle, the P_{rot} was within 5% of one flagged as due to contamination in a different cycle, we removed that P_{rot} from our sample as well. This resulted in the removal of 69, 58, and 82 P_{rot} that were not removed by previous steps from our samples for Cycles 1, 3, and 5, respectively.

⁹We use “variability” here to recognize that any periodicity we measure in these light curves is unlikely to be due to rotation.

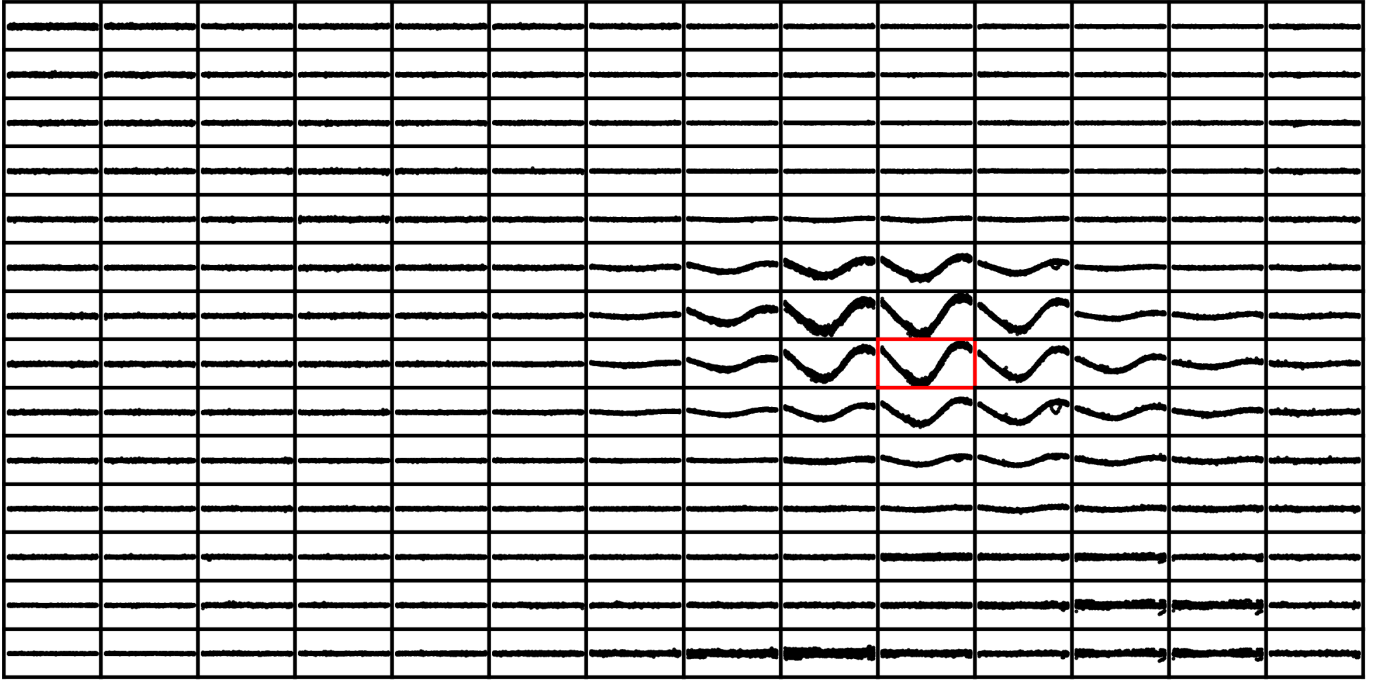


Figure 7. Light curves produced for each pixel in Figure 6 phase-folded on a period of 2.10 days, the period of the classical Cepheid Gaia DR3 5340164256296564736. The light curve for the pixel hosting the Cepheid is highlighted with a red frame. The 2.10 day signal is dominant in the light curve extracted from that pixel, as expected, but also in those extracted from many surrounding pixels. The y-axes of these plots share a flux scale, demonstrating the relative strength of the 2.10 day signal.

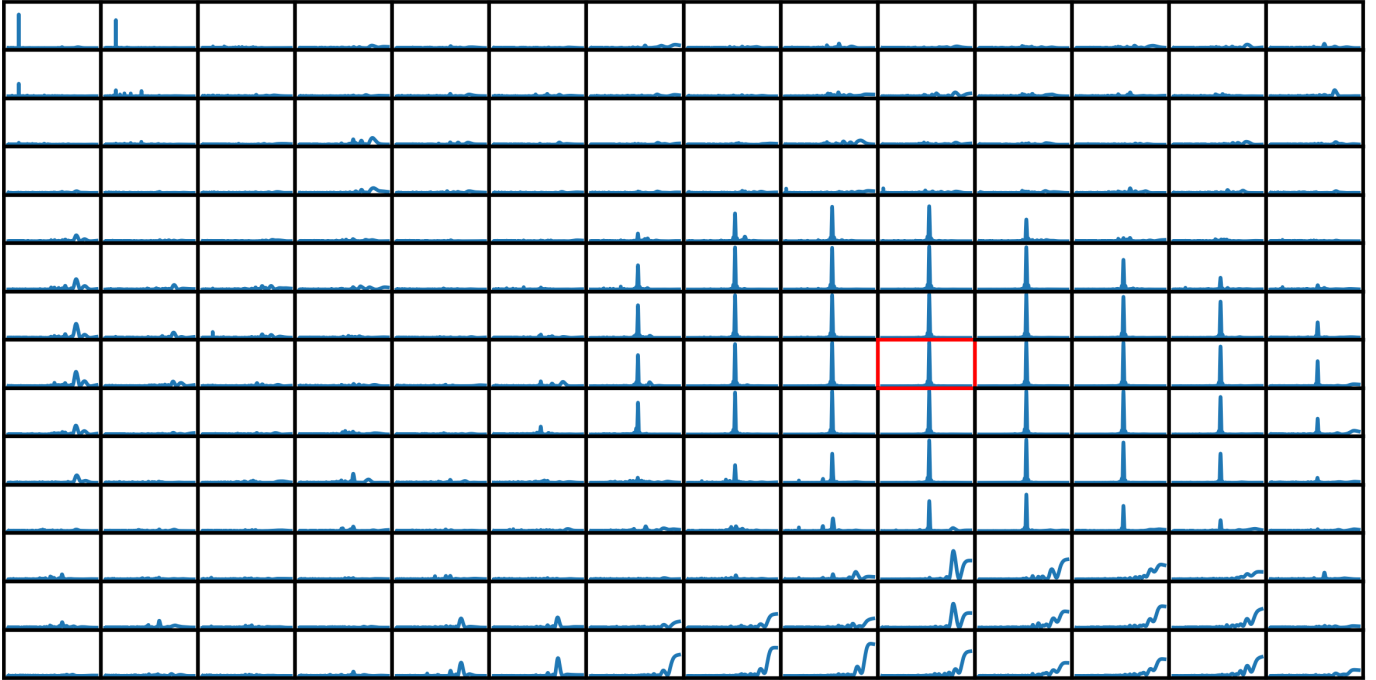


Figure 8. Periodograms produced for the light curves shown in Figure 7. X-axes are logarithmically spaced periods and y-axes are periodogram powers. The periodogram for the pixel hosting Gaia DR3 5340164256296564736 is highlighted with a red frame. The impact of this bright Cepheid on measurements from neighboring pixels is very evident, with its 2.10 day signal being the strongest signal measured in periodograms corresponding to pixels as far removed as $\approx 1'$.

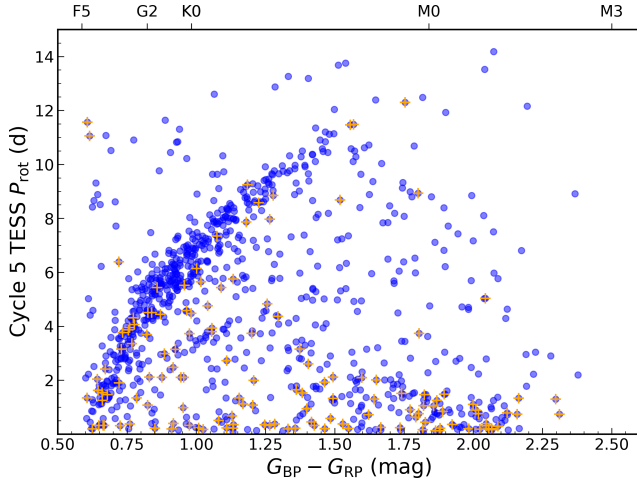


Figure 9. TESS Cycle 5 CPD. All the periods shown here have powers above the threshold for this cycle. P_{rot} measurements identified for removal due to source confusion either by GVC objects or by other cluster members are marked with orange crosses. A significant fraction of these P_{rot} are <0.5 days, faster than we would expect for e.g., stars earlier than mid-K at this age (see D. J. Fritzewski et al. 2021a).

Figure 9 shows the impact of removing P_{rot} contaminated either by GVC sources or by other cluster members on the P_{rot} distribution for Cycle 5.

3.4. Correcting P_{rot} Measurements That Result From Half-Period Harmonics

Based on the half-period sequences of the slow-rotating sequences that appear in the pre-analysis CPDs in the left column of Figure 3, and on cases where we measured a period \approx half that reported in D. J. Fritzewski et al. (2021a) for a given target (as seen in Figure 12 and discussed in Section 4.1), we identified and corrected P_{rot} measurements resulting from half-period harmonics of the true period in our data. The availability of data from multiple TESS cycles was useful for identifying cases where we incorrectly assigned to a star half of its true P_{rot} . Observations in Cycles 1, 3, and 5 were taken $\gtrsim 2$ years apart, long enough that the star spot distribution responsible for modulating our targets' light curves can evolve.¹⁰ This may change the shape of the light curves, resolving confusion about which period is the real one and which is the harmonic.

¹⁰We do not expect the actual P_{rot} to change on this timescale. The evidence from K2 data for the older Praesepe cluster is that while many light curves evolve on a very similar timescale, the derived P_{rot} measurements are remarkably stable (R. Rampalli et al. 2021).

Moreover, as shorter P_{rot} are easier to detect in TESS data, in cases where we obtained a P_{rot} for a star double that in one cycle relative to another, it is likely that the shorter P_{rot} is not the true period. We searched for $P_{\text{rot}} < 7.5$ days, when doubled, are $<5\%$ different from a P_{rot} measurement for the same star in another cycle. We flagged these shorter P_{rot} as potential harmonics of the true periods.

Our two-term LS periodograms also helped with the identification of these cases. The two-term periodograms use an additional sinusoidal term when fitting the data, allowing for more robust P_{rot} detection in some cases where the starspot distribution creates a signal that is more complex than can be represented by a single sine wave (e.g., “double dipping,” G. Basri & H. T. Nguyen 2018). For each measurement, we compared the one-term and two-term LS periodograms.

In cases where we measure the half-period harmonic of the true P_{rot} for a target, the true P_{rot} can appear as a lower-order peak in the one-term periodogram. We therefore flagged cases where the primary peak of the two-term periodogram matched the secondary peak of the one-term periodogram, provided that this secondary peak was at a period double that of the primary peak in the one-term periodogram. Figure 10 shows a periodogram comparison that resulted in such a flag that helped provide evidence to correct a harmonic P_{rot} measurement of a target for Cycle 5.

For measurements that were flagged in both the periodogram comparison as well as the comparison with the measured P_{rot} from other cycles, we replaced our original P_{rot} measurement with that determined by the primary peak in the two-term LS periodogram. This resulted in the replacement of 15, 15, and 31 measurements for TESS Cycles 1, 3, and 5, respectively. In Figure 11, we show the P_{rot} we corrected in this manner in Cycle 5.

3.5. Assessing the Impact of Applying Our Criteria

The cumulative effect of the steps described above to remove or correct spurious P_{rot} measurements can be seen in the right column of Figure 3. Applying the periodogram power requirement removed by far the most measurements from the original CPD. Among the remaining high-power measurements, hundreds more were identified for removal due to source confusion, a necessary step for producing a P_{rot} catalog for rich and relatively distant clusters like NGC 3532.

Each CPD on the left side of Figure 3 includes many spurious measurements with $P_{\text{rot}} < 1$ day that were removed in this step, as can be seen in the corresponding cleaned CPDs on the right. The changes in the P_{rot}

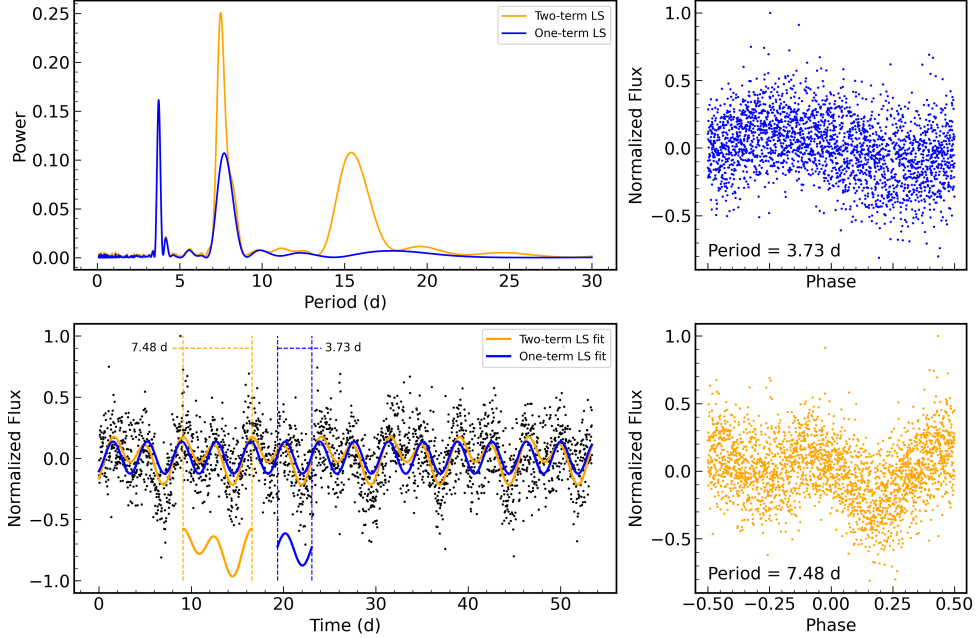


Figure 10. An example of a star for which using the two-term LS led to a period correction. The one- and two-term LS periodograms are shown at the top left. The corresponding best-fit LS models at the highest power period for each periodogram are plotted with the Cycle 5 light curve (bottom left). The location of the secondary peak in the one-term periodogram (7.48 days) matches the location of the primary peak in the two-term periodogram (3.73 days). This corresponds to a P_{rot} that is approximately double that measured using the location of the primary peak in the one-term periodogram (3.73 days). The original measurement at 3.73 days is a half-period harmonic of the true period and was corrected to 7.48 days. The top right panel shows the light curve phase-folded on the original P_{rot} measurement, while the bottom right panel is the light curve phase-folded on the corrected measurement. The varying amplitude of the signal (i.e., the “double dipping” causing the harmonic measurement) is evident in the bottom right, phase-folded light curve and is accurately modeled by the two-term periodogram.

distribution due to the removal of measurements due to systematics, particularly in Cycle 1, is also apparent in comparing the CPDs, as is the impact of our efforts to identify and correct half-period aliases.

Most importantly, several hundred high-confidence P_{rot} measurements were preserved in each cycle, as evidenced by the well-defined and well-populated sequences of slowly rotating stars in the CPDs in Figure 3 and the remaining P_{rot} measurements that agree with those from D. J. Fritzewski et al. (2021a). This gave us confidence that we could construct a robust, expanded rotational catalog for NGC 3532 based on these TESS data.

A summary of the number of P_{rot} measurements removed by each step of the quality assessment of our measurements is shown in Table 2.

4. EXPANDING THE ROTATIONAL CENSUS FOR NGC 3532

4.1. *Revisiting the D. J. Fritzewski et al. (2021a) P_{rot} Catalog*

We compared our automatically measured P_{rot} prior to any quality cuts to those in the D. J. Fritzewski et al. (2021a) catalog to assess their robustness. The results for each cycle are shown in the left column of Figure 12,

Table 2. P_{rot} measurements identified for removal^a

	Cycle 1	Cycle 3	Cycle 5
Targets observed	1357	1054	1341
$P_{\text{rot}} > 15$ d	91	28	20
Low power	377	308	395
Systematic error	68	10	N/A
Blending: GVC	94	85	115
Blending: Members	69	58	82
Unconfirmed rapid P_{rot}	15	15	31
Remaining measurements	643	550	698

^a Rows 2–7 represent the number of P_{rot} measurements identified for removal by each quality criterion after measuring P_{rot} for each observation of each target. The numbers in these rows are those P_{rot} measurements identified for removal that were not previously flagged for removal by any criterion represented by an above row.

where we limit the comparison to stars for which we measured a $P_{\text{rot}} < 15$ days.

About half of our P_{rot} measurements from each TESS cycle differ by <15% from those from D. J. Fritzewski

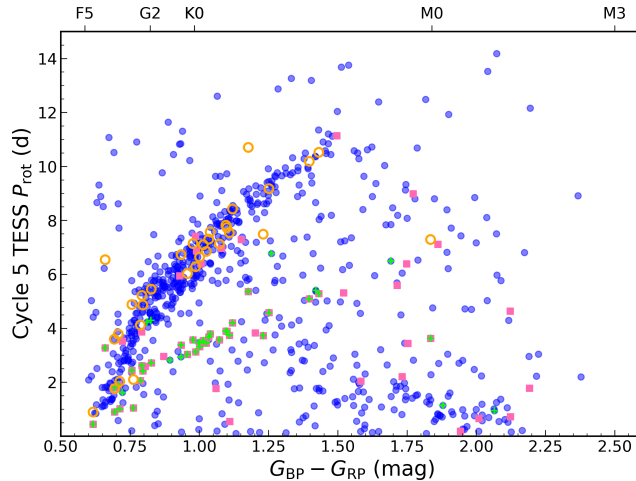


Figure 11. TESS Cycle 5 CPD. Stars for which we measured twice the P_{rot} measured for Cycle 5 (using the standard LS periodogram) in a different TESS cycle are marked with a green cross. P_{rot} measurements identified as potential harmonic measurements using a comparison between one-term and two-term LS periodogram are marked with pink squares. Where both these criteria are met for a given P_{rot} measurement, we replaced our original measurement with the two-term LS measurement. The corrected measurements are marked with orange circles.

et al. (2021a). The agreement is 48% for Cycle 1 (117/245 periods), 44% for Cycle 3 (101/229), and 54% for Cycle 5 (139/258); our P_{rot} measurements that agree with the literature appear as the red circles in Figure 3. When we combined the results for all three cycles, this overall recovery rate increased to 69%—meaning that we recovered the D. J. Fritzewski et al. (2021a) P_{rot} 7/10 times in at least one of the TESS cycles.

Those agreement rates do not tell the full story, however: we were more likely to recover the photometric P_{rot} measurements from D. J. Fritzewski et al. (2021a). The agreement rates between our measurements and these authors' highest-confidence photometric P_{rot} (the class 1 periods) were 53% (45/85), 51% (40/78), and 58% (52/89) for Cycles 1, 3, and 5 respectively. These agreement rates dropped to 44% (25/57), 40% (20/50), and 53% (31/59) for the class 2 photometric P_{rot} , and dropped again, to 42% (37/88), 38% (32/84), and 48% (45/94), for the class 3 (activity-informed) P_{rot} . Interestingly, the agreement rates for the class 0 P_{rot} (potential aliases) was 67% (10/15), 53% (9/17), and 69% (11/16) for Cycles 1, 3, and 5 respectively.

The left column of Figure 12 suggests that where our measurements and those of D. J. Fritzewski et al. (2021a) disagreed significantly, it is because our TESS measurements preferentially returned relatively short

periods, as expected given the length of a sector. It also shows that we measured dozens of periods that fall on or near the 1:2 harmonic line, indicating again that harmonic P_{rot} measurements appear in our sample and should be corrected where sufficient evidence is present.

Following our analysis removing spurious measurements from our P_{rot} sample, we retained measurements for 179 stars with existing P_{rot} in the D. J. Fritzewski et al. (2021a) catalog. We recovered the P_{rot} from their catalog in at least one TESS cycle for 143 of these stars (80%). The agreement rates between our measurements in each TESS cycle and the literature periods improved significantly following our analysis, as can be seen in the panels on the right side of Figure 12.

The post-analysis agreement rates between our measurements and these authors' class 1 periods improved to 86% (36/42), 78% (38/49), and 87% (46/53) for Cycles 1, 3, and 5 respectively. The agreement rates for the class 2 photometric P_{rot} improved to 79% (20/27), 65% (17/26), and 79% (23/29), and for the class 3 (activity-informed) P_{rot} , improved to 67% (30/45), 64% (27/42), and 70% (31/44). The agreement rates for the class 0 P_{rot} (potential aliases) also improved to 80% (4/5), 56% (5/9), and 78% (7/9) for Cycles 1, 3, and 5, respectively.

A. W. Boyle et al. (2025) performed a comparison of TESS-derived P_{rot} measured from CPM light curves and P_{rot} from a K2 benchmark sample. After applying quality cuts to remove stars with significant photometric contamination and binaries, these authors found that $\gtrsim 80\%$ of the TESS $P_{\text{rot}} \leq 10$ days agree with those obtained from K2 data, similar to our rate of agreement with the D. J. Fritzewski et al. (2021a) class 1 P_{rot} .

Many of the cases where we failed to recover the P_{rot} from the D. J. Fritzewski et al. (2021a) catalog are for slow rotators and/or for relatively faint stars, whose P_{rot} are particularly difficult to obtain with TESS data. For the 36 stars for which we measured a P_{rot} that we did not flag as problematic and that disagrees by more than 15% with the D. J. Fritzewski et al. (2021a) P_{rot} , the median magnitude is $G = 15.4$ mag.

Finally, there may be a small number of cases where we report an accurate P_{rot} that does not agree with the literature. For example, there are stars for which the P_{rot} we measure is approximately twice that measured by D. J. Fritzewski et al. (2021a), as shown by the points falling on or near the 2:1 line in the panels of Figure 12. It is possible that the spot distribution on the star at the time of observation caused these authors to measure the harmonic P_{rot} .

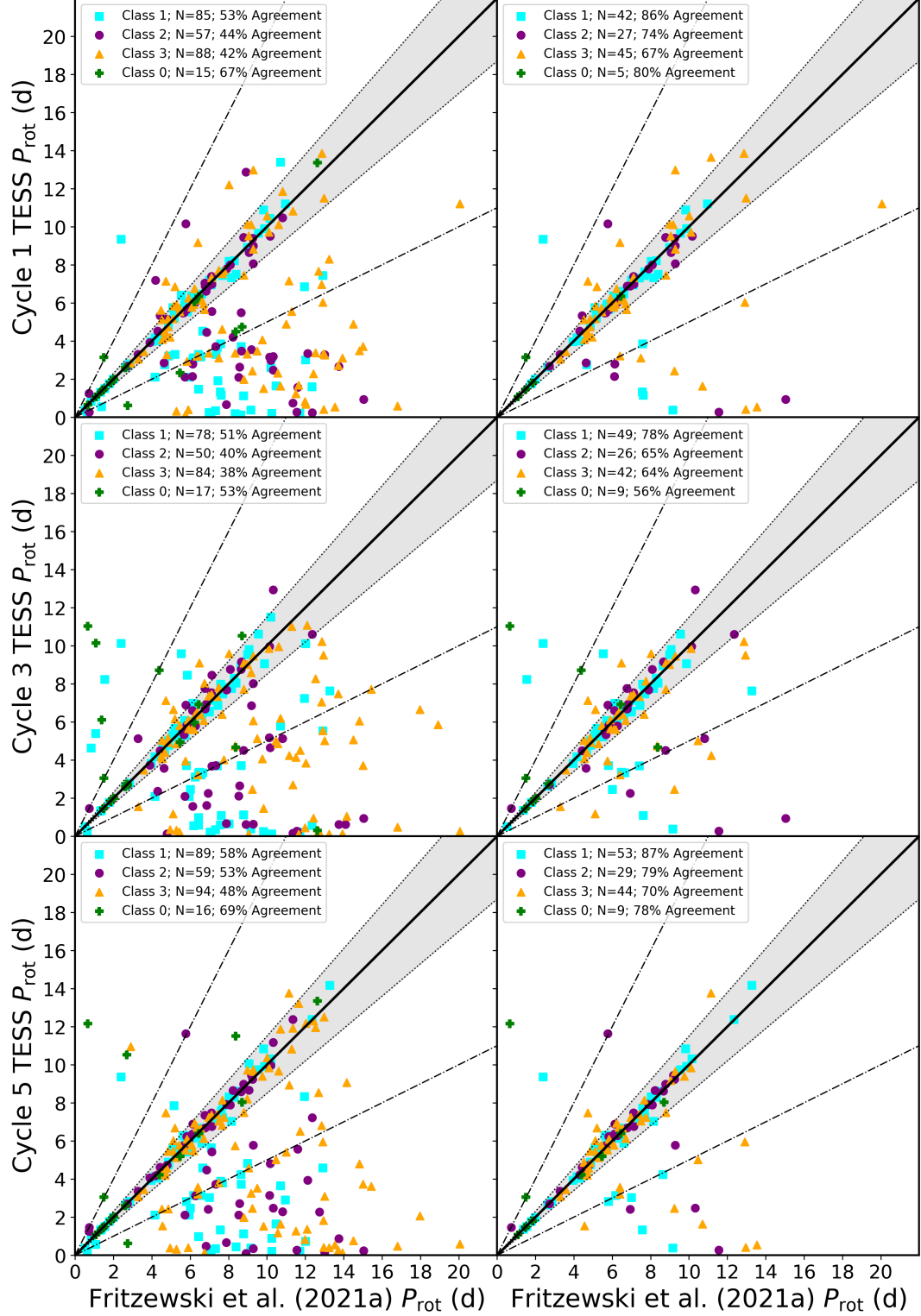


Figure 12. Comparisons of the P_{rot} measured using TESS light curves from Cycles 1, 3, and 5 with those from D. J. Fritzewski et al. (2021a) before (left) and after (right) our analysis removing our erroneous measurements. The shaded region indicates a difference of $\leq 15\%$ between the TESS and literature P_{rot} values, which we take to be an agreement in the measurements. We also include 2:1 and 1:2 lines to indicate possible harmonic or subharmonic measurements. The classification assigned to each P_{rot} measurement in D. J. Fritzewski et al. (2021a) is indicated with a different symbol. Even before analyzing our results, we have a high P_{rot} recovery rate (50–60%) for the high-confidence (class 1) measurements from D. J. Fritzewski et al. (2021a), shown as filled cyan squares. Our initial agreement rate for lower-confidence measurements—especially those obtained using activity as a prior (class 3; filled orange triangles)—is systematically lower ($\approx 40\text{--}50\%$). Our analysis of cases where our measurements differ significantly from those of D. J. Fritzewski et al. (2021a) allows us to improve our recovery rate, so that it reaches $\gtrsim 80\%$ for the class 1 P_{rot} , while other classes of P_{rot} measurements saw slightly smaller improvements in agreement rate.

4.2. The new NGC 3532 P_{rot} catalog

Having identified likely inaccurate P_{rot} measurements made using data from each TESS cycle, we consolidated the multiple P_{rot} measurements of the same stars into a final set of P_{rot} . Cases where the periods do not agree from cycle to cycle were not uncommon. For example, of the 179 stars from [D. J. Fritzewski et al. \(2021a\)](#) for which we retained P_{rot} measurements following our analysis, we measured a P_{rot} that agreed with the literature value for one TESS cycle and disagreed for another for 39 stars (22%!).

Where P_{rot} measurements obtained from multiple cycles survived our quality cuts, we calculated the median P_{rot} and identified which measurements agreed with this value within 10%. For stars with multiple measurements that agreed with the median value, we recalculated the median using only those measurements, and reported it as the final P_{rot} for the target. If none of the measurements were within 10% of the median P_{rot} , we reported the longest P_{rot} as the final P_{rot} . We reasoned that this would generally select the true P_{rot} , since rapid P_{rot} are relatively easily detected and are more likely to be measured with multiple observations. For stars with only one P_{rot} measurement after our quality cuts, we simply reported that P_{rot} as the final P_{rot} .

We classified our final P_{rot} measurements according to the number of agreeing measurements used to arrive at the final measurement. Final P_{rot} based on three agreeing measurements were our highest confidence P_{rot} , and classified as Quality 3. Those based on two agreeing measurements are Quality 2, and those based on only one P_{rot} measurement are classified as Quality 1.

In this manner, we created an expanded P_{rot} catalog that includes 885 members of NGC 3532: 261 with Quality 3 P_{rot} , 309 with Quality 2, and 315 with Quality 1. In Figure 13, we show the CPDs for each quality group, as well as the CPD containing all the final P_{rot} measurements. In that CPD (bottom right panel), we also highlight the 228 stars with HDBSCAN membership probabilities $<50\%$ in [E. L. Hunt & S. Reffert \(2023\)](#). Many of these stars have P_{rot} measurements that fall on the slow-rotating sequence for NGC 3532, suggesting that they are part of the coeval cluster population. We are therefore able to confirm these at least as likely cluster members.

The CPD in the bottom right panel of Figure 13 containing all of our final P_{rot} measurements features a well-populated slow-rotating sequence as well as a fast-rotating sequence that includes K stars still converging onto the slow sequence. This is consistent with the findings of [D. J. Fritzewski et al. \(2021a\)](#) and expected for a cluster of the age of NGC 3532. Most of our new P_{rot}

measurements fall in regions of the CPD already populated with measurements from [D. J. Fritzewski et al. \(2021a\)](#). We added P_{rot} measurements for mid-to-late F stars on the slow-rotating sequence for which there were previously none. The slow-rotating sequence defined by our P_{rot} measurements does not extend to include M dwarfs although they are present in the [D. J. Fritzewski et al. \(2021a\)](#) catalog. This is the result of the limitations of TESS in measuring P_{rot} for slow-rotators and faint stars. Meanwhile, the relatively small population of fast-rotating G stars that fall beneath the slow-rotating sequences in the CPDs in Figure 13 are not likely to be accurate for a cluster of the age of NGC 3532 and might be the result of unidentified cases of photometric blending, or else are tidally-interacting binaries.¹¹

We repeated our comparison with P_{rot} from [D. J. Fritzewski et al. \(2021a\)](#), now using our final P_{rot} measurements and comparing agreement rates for our quality classifications. The resulting P_{rot} comparison plot is shown in Figure 14. The overall agreement between the two sets of measurements is 77%, but it does vary significantly according to our quality classifications: it is 87% for our Quality 3 periods, and drops to 77% and 69% for our Quality 2 and 1 periods respectively.¹² These agreement rates serve as an estimate of an upper limit of the proportion of our P_{rot} measurements that are accurate in each quality group. We are therefore more confident in P_{rot} measurements confirmed with multiple observations and suspect that most of the remaining disagreement is caused by blended signals not recognized by our procedure.

In Figure 15, we show a CPD using P_{rot} from [D. J. Fritzewski et al. \(2021a\)](#) and highlight the 41 cases where our final measurement disagrees by $>15\%$ with the literature P_{rot} for the same star. Generally, we are more likely to measure relatively rapid P_{rot} due to their systematically higher powers in LS periodograms. Some erroneous rapid P_{rot} measurements persist in our final

¹¹[D. J. Fritzewski et al. \(2021a\)](#) provides a detailed discussion of the morphology of the CPD for NGC 3532 and comparisons to some existing semi-empirical models. [L. G. Bouma et al. \(2023\)](#) and [P. R. Van-Lane et al. \(2025\)](#) place the period data for NGC 3532 in the context of many other open clusters and use those data to build new empirical gyrochronology models (`gyro-interp` and `ChronoFlow`, respectively).

¹²Although we recovered P_{rot} for 80% of our remaining targets post-analysis with existing measurements from [D. J. Fritzewski et al. \(2021a\)](#) in at least one TESS cycle, our final P_{rot} selection process was not informed by existing P_{rot} measurements. For five stars, the final P_{rot} we selected does not agree with the literature P_{rot} even though we measured P_{rot} that agreed with the existing measurement for one TESS cycle.

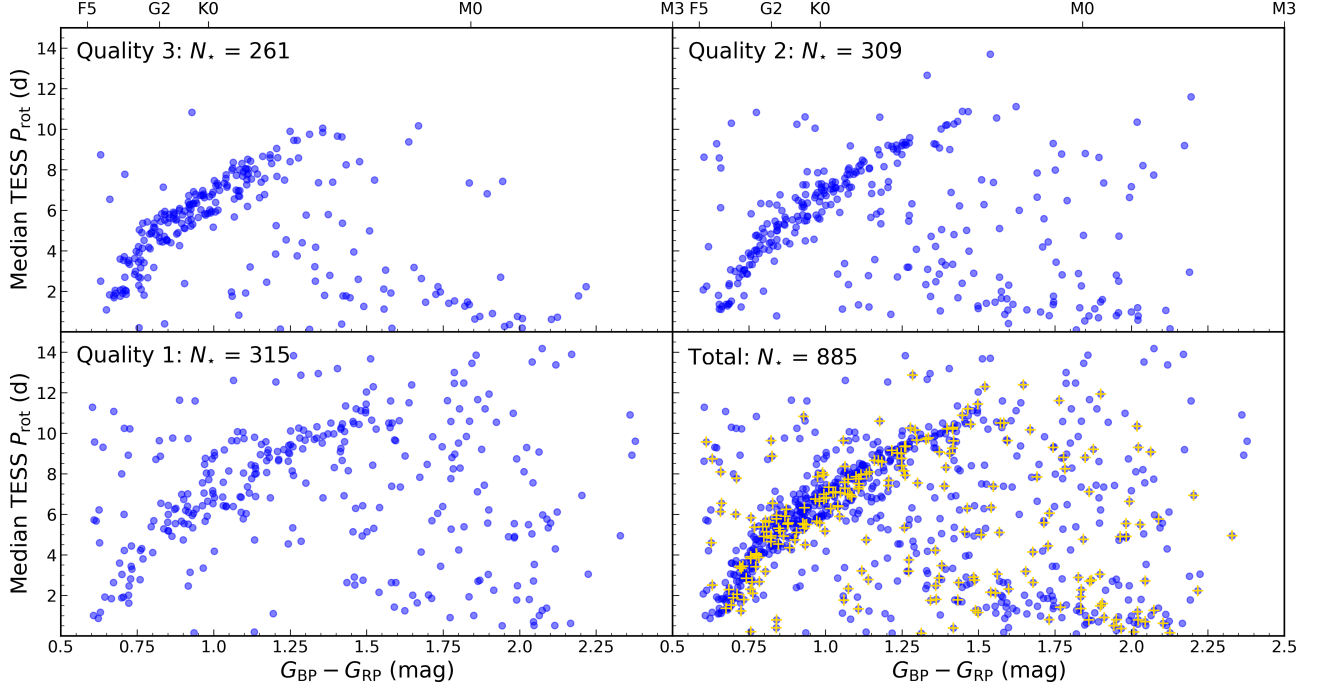


Figure 13. CPDs for NGC 3532 based on quality classification of the final P_{rot} measurement reported for each star. Measurements classified as Quality 3 represent our highest confidence P_{rot} , where the measured period was consistent across all three TESS cycles. Quality 2 P_{rot} are measurements that agreed in two TESS cycles, and Quality 1 P_{rot} were measured in only one cycle, sometimes corresponding to the longest P_{rot} measured when measurements in multiple cycles disagreed. In total, we make new P_{rot} measurements for 885 stars, all of which are plotted in the bottom right CPD. The yellow crosses in that CPD correspond to the 228 stars that have HDBSCAN membership probabilities of $<50\%$ as indicated by E. L. Hunt & S. Reffert (2023) and for which we make new P_{rot} measurements. Many of these lower-probability members fall on the slow-rotating sequence, suggesting that they are a part of the coeval NGC 3532 population and are likely cluster members.

catalog, most likely due to unidentified cases of photometric blending. Our recovery of P_{rot} measurements for slower rotators is comparatively low presumably due to a combination of this contamination, the fact that slower rotators tend to be relatively faint, and that, as mentioned, TESS has limited ability to detect variability on longer time scales. Figure 14 also suggests that we may not have successfully identified all of the harmonic measurements we made since some inaccurate measurements are \approx half the P_{rot} from D. J. Fritzewski et al. (2021a).

Our recovery rate of D. J. Fritzewski et al. (2021a) P_{rot} is highest for these authors' highest confidence measurements, those directly measured from photometry. Similarly, the agreement rate between our P_{rot} and those from D. J. Fritzewski et al. (2021a) is highest for our highest confidence (Quality 3) measurements at 87%. We conclude that this justifies using P_{rot} measured from TESS observations to build P_{rot} catalogs for NGC 3532 and other crowded open clusters. However, this must be done with appropriate caution to identify inaccurate P_{rot} measurements, especially for fainter stars and slower rotators, and ideally using multiple TESS observations to validate P_{rot} measurements.

While our recovery rate is lower for lower-confidence D. J. Fritzewski et al. (2021a) P_{rot} measurements, we did recover a substantial fraction of the P_{rot} these authors measured using predictions based on a target's chromospheric activity, underscoring the usefulness of this approach. In general, however, many of these lower-confidence P_{rot} are for stars for which it is difficult to measure P_{rot} with TESS. And our efforts to produce our expanded P_{rot} catalog for NGC 3532 are successful in identifying most of our inaccurate measurements for these targets.

In Table 3, we provide a description of the columns in our final P_{rot} catalog for NGC 3532.

5. CONCLUSION

TESS provides us with the ability to measure P_{rot} for low-mass stars across most of the sky. However, TESS's large pixels mean that blending and source confusion are a concern when constructing P_{rot} catalogs for relatively distant and/or crowded fields.

We used the relatively young, relatively distant, and rich open cluster NGC 3532 as a test case for a procedure for removing inaccurate P_{rot} measurements from an

Table 3. Columns in Our NGC 3532 Rotation Catalog

Column	Description
1	Gaia DR3 source designation
2	HDBSCAN membership probability (E. L. Hunt & S. Reffert 2023)
3, 4	R.A., decl. at Epoch = 2016.0
5, 6	Parallax and 1σ uncertainty
7	Gaia DR3 G magnitude
8	Gaia DR3 color ($G_{\text{BP}} - G_{\text{RP}}$)
9	Gaia DR3 Re-normalized Unit Weight Error
10	Binary flag ($\text{RUWE} > 1.4$) ^a
11	TESS-based rotation period P_{rot}
12	P_{rot} quality classification ^b
13, 14	P_{rot} and periodogram power (Cycle 1) ^c
15, 16	P_{rot} and periodogram power (Cycle 3) ^c
17, 18	P_{rot} and periodogram power (Cycle 5) ^c
19, 20, 21	Low power flag (Cycles 1, 3, and 5) ^a
22, 23, 24	Source confusion flag (Cycles 1, 3, and 5) ^a
25, 26	Systematic error flag (Cycles 1 and 3) ^a
27, 28, 29	Corrected harmonic period flag (Cycles 1, 3, and 5) ^a
30, 31, 32	Vanished rapid period flag (Cycles 1, 3, and 5) ^a
33	Literature P_{rot} (D. J. Fritzevski et al. 2021a) ^d
34	Literature P_{rot} class (D. J. Fritzevski et al. 2021a) ^d

NOTE—The contents of this table are published as a machine-readable table in the electronic edition of the Journal.

^aColumns for data flags use zero to represent no flag and one to represent a flag.

^bThe quality classification for a given TESS rotation period is equal to the number of TESS observations used to confirm that rotation period measurement.

^cColumns for rotation periods and periodogram powers for individual TESS cycles use zero to represent no available data and negative values to represent values flagged for removal.

^dColumns with data from the existing rotation period catalog for NGC 3532 (D. J. Fritzevski et al. 2021a) use -1 to represent no available data.

automatically generated period catalog produced from TESS data. While we compared our results to the existing D. J. Fritzevski et al. (2021a) P_{rot} catalog for the cluster to test our approach’s usefulness and reliability, ultimately we relied on data from TESS and Gaia to evaluate our periods, and our approach can therefore be applied to clusters without existing rotation catalogs.

The primary source of inaccurate P_{rot} measurements that seem to be of good quality is the presence of neighboring variable sources with comparatively strong signals that cause photometric blending in target light curves. By identifying stars with such neighbors and removing our measurements of their P_{rot} from our rotation catalog, we were able to produce a reliable, expanded period catalog for NGC 3532 that more than triples the size of the sample for this cluster: D. J. Fritzevski et al. (2021a) published P_{rot} measurements for 279 stars, and

our catalog includes 885 stars, 706 of which did not previously have a P_{rot} measurement.

We assessed our approach by comparing our P_{rot} measurements to those obtained by D. J. Fritzevski et al. (2021a) several times. The first was after running a standard Lomb-Scargle-based search for periods in all of the TESS data available for the E. L. Hunt & S. Reffert (2023) cluster members. We found that we could recover accurate (within 15%) P_{rot} for 69% of the D. J. Fritzevski et al. (2021a) stars in at least one cycle of TESS data before any analysis of the quality of our measurements. Post this analysis, the overall agreement rate between our measurements increased to 77%, but it is 86% for the highest quality D. J. Fritzevski et al. (2021a) P_{rot} measurements and 87% for our own highest-confidence measurements, a remarkable result given the apparent challenges a crowded field like that of NGC 3532 poses to TESS.

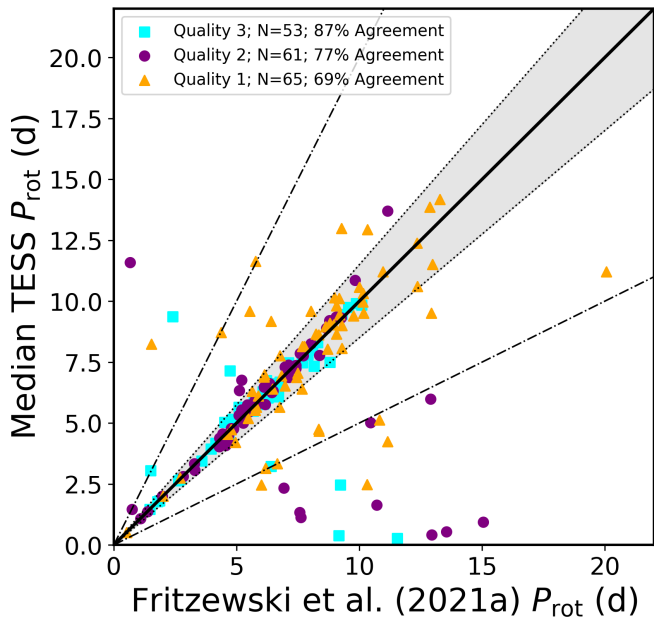


Figure 14. Comparison of our final P_{rot} measurements with those from D. J. Fritzewski et al. (2021a). Different symbols are given to indicate the quality classification we assigned our P_{rot} measurements. Our higher-confidence P_{rot} measurements, which are validated with observations from multiple TESS cycles (filled cyan squares, 3 cycles; filled purple circles, 2) have higher agreement rates with the measurements from D. J. Fritzewski et al. (2021a).

In our final catalog, there were 41 stars for which our measured P_{rot} disagreed with the P_{rot} of D. J. Fritzewski et al. (2021a) by more than 15%. For each of these stars, we inspected the light curves and periodograms produced from the targets' pixels and surrounding pixels to understand what might be causing inaccurate measurements that persist despite our attempts to filter them out. In many of these cases, there was a signal from a neighboring source that interfered with the measurement for our target. In some cases, this led to a measurement of variability that is clearly accurate for a nearby source and not for our target. In other cases, the photometric contamination is sufficiently complicated that it is not clear if the period reported is accurate for any nearby source. As discussed in Section 3.5, we removed from our catalog measurements caused by source confusion only if we were able to identify the true source of the detected variability. This prevented us from identifying every case of photometric contamination in our catalog. There also may remain a few cases where we measured the harmonic of the true P_{rot} and did not find enough evidence to correct this measurement in our analysis. This suggests that inaccurate P_{rot} measurements remain in

our expanded catalog, particularly for (relatively) slow rotators and faint stars.

We benefited from having three cycles' worth of TESS data for NGC 3532, which gave us three separate opportunities to measure P_{rot} for many of our targets. Interestingly, our analysis of the data from the three cycles did not always return the same P_{rot} for our targets. The changing orientation of the telescope between cycles causes different pixel geometries relative to the field, which can impact our measurements. There were also clear systematics present in one or the other of the cycles. As a result, for some stars it was possible to measure an accurate P_{rot} for a target using FFIs from one TESS cycle, but not another. We used the agreement in our measurements between cycles to assign a quality to our P_{rot} .

In some cases, we removed from our sample P_{rot} measurements that agreed with the existing measurement from D. J. Fritzewski et al. (2021a) for a given star. This occurred most frequently due to our largest quality cut: the periodogram power threshold. Across the three studied TESS cycles, we removed 209 P_{rot} measurements for stars with existing measurements from the literature catalog with this quality cut. Of these measurements, 50 agreed with that from the literature within 15%. While 3/4 of the measurements we removed with this quality cut are spurious, it may be possible to recover more accurate low-power measurements, especially using additional observations as TESS continues to survey the sky.

NGC 3532 was recently observed in TESS Cycle 7 and will be observed again in Cycles 8 and 9. In Cycle 9, NGC 3532 will be observed in three consecutive sectors, possibly enabling measurement of higher-confidence P_{rot} for slow rotators. A re-analysis of our catalog after these observations should result in a refinement and possibly an expansion of our period catalog. As is, the catalog presented here is one of the largest assembled for an open cluster, and should contribute to efforts to calibrate gyrochronology for low-mass main-sequence stars.

Further development and application of the strategies introduced here will allow for more reliable measurement of P_{rot} in distant, crowded clusters that continue to be observed by TESS. This opens the possibility of producing expansive P_{rot} catalogs for open clusters (or other co-moving, coeval structures) at unstudied or understudied ages and metallicities, thereby contributing new benchmarks to studies of gyrochronology.

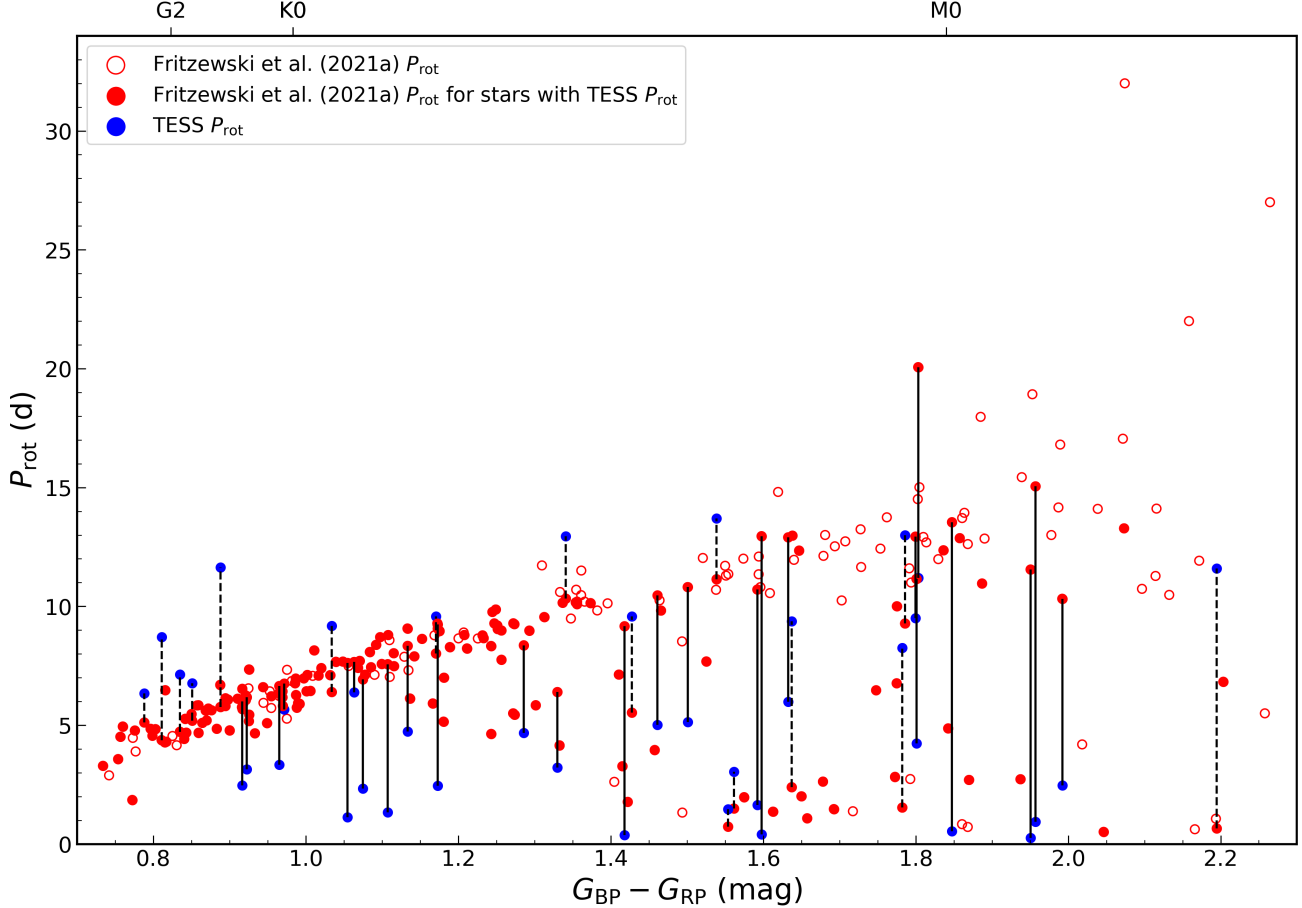


Figure 15. CPD for NGC 3532 comparing the P_{rot} reported by D. J. Fritzewski et al. (2021a) and our measurements. The filled red circles are literature P_{rot} for stars for which we obtained a P_{rot} , while the open red circles are literature P_{rot} for stars for which we did not. The filled blue circles are our 41 newly measured P_{rot} that disagreed by $>15\%$ with the D. J. Fritzewski et al. (2021a) P_{rot} . Black lines connect our measurements and the D. J. Fritzewski et al. (2021a) periods when our P_{rot} is shorter. Dashed lines are used for the opposite case. In most cases where the P_{rot} measurements disagree significantly, we measured a P_{rot} that is much more rapid than that in D. J. Fritzewski et al. (2021a), suggesting that a fraction of our measurements remain impacted by blending.

ACKNOWLEDGMENTS

We thank the anonymous reviewer for their careful reading and comments that improved the manuscript.

This work was supported by NSF Astronomy & Astrophysics Grant AST-2009840 and NASA TESS GI grants No. 80NSSC22K0299 (program ID G04217), 80NSSC23K0369 (program ID G05157), 80NSSC23K0370 (program ID G05028), and 80NSSC24K0501 (program ID G06163). M.A.A. acknowledges support from a Fulbright U.S. Scholar grant co-funded by the Nouvelle-Aquitaine Regional Council and the Franco-American Fulbright Commission. M.A.A. also acknowledges support from a Chrétien International Research Grant from the American Astronomical Society.

This paper includes data collected by the TESS mission, which are publicly available from the Mikulski

Archive for Space Telescopes (MAST). Funding for the TESS mission is provided by NASA’s Science Mission directorate. The TESS data used in this paper can be found in MAST: [10.17909/0cp4-2j79](https://doi.org/10.17909/0cp4-2j79).

This work has made use of data from the European Space Agency (ESA) mission Gaia,¹³ processed by the Gaia Data Processing and Analysis Consortium (DPAC).¹⁴ Funding for the DPAC has been provided by national institutions, in particular the institutions participating in the Gaia Multilateral Agreement. This research also made use of public auxiliary data provided by ESA/Gaia/DPAC/CU5 and prepared by Carine Babusiaux.

¹³<https://www.cosmos.esa.int/gaia>

¹⁴<https://www.cosmos.esa.int/web/gaia/dpac/consortium>

The Digitized Sky Surveys were produced at the Space Telescope Science Institute under U.S. Government grant NAG W-2166. The images of these surveys are based on photographic data obtained using the Oschin Schmidt Telescope on Palomar Mountain and the UK Schmidt Telescope. The plates were processed into the present compressed digital form with the permission of these institutions.

This research has also made use of NASA's Astrophysics Data System, and the VizieR (F. Ochsenbein et al. 2000) and SIMBAD (M. Wenger et al. 2000) databases operated at CDS, Strasbourg, France.

Facilities: TESS, Gaia

Software: astropy (Astropy Collaboration et al. 2013, The Astropy Collaboration et al. 2018), astroquery (A. Ginsburg et al. 2019), Matplotlib (J. D. Hunter 2007), NumPy (C. R. Harris et al. 2020), SciPy (E. Jones et al. 2001), TESScut (C. E. Brasseur et al. 2019), unpopular (S. Hattori et al. 2022), lightkurve (Lightkurve Collaboration et al. 2018)

REFERENCES

Agüeros, M. A., Curtis, J. L., Núñez, A., et al. 2025, *ApJ*, 993, 144, doi: [10.3847/1538-4357/ae03a3](https://doi.org/10.3847/1538-4357/ae03a3)

Anthony, F., Núñez, A., Agüeros, M. A., et al. 2022, *AJ*, 163, 257, doi: [10.3847/1538-3881/ac6110](https://doi.org/10.3847/1538-3881/ac6110)

Astropy Collaboration, Robitaille, T. P., Tollerud, E. J., et al. 2013, *A&A*, 558, A33, doi: [10.1051/0004-6361/201322068](https://doi.org/10.1051/0004-6361/201322068)

Barnes, S. A. 2003, *ApJ*, 586, 464, doi: [10.1086/367639](https://doi.org/10.1086/367639)

Barnes, S. A. 2007, *ApJ*, 669, 1167, doi: [10.1086/519295](https://doi.org/10.1086/519295)

Basri, G., & Nguyen, H. T. 2018, *ApJ*, 863, 190, doi: [10.3847/1538-4357/aad3b6](https://doi.org/10.3847/1538-4357/aad3b6)

Borucki, W. J., Koch, D., Basri, G., et al. 2010, *Science*, 327, 977, doi: [10.1126/science.1185402](https://doi.org/10.1126/science.1185402)

Bouma, L. G., Hartman, J. D., Bhatti, W., Winn, J. N., & Bakos, G. Á. 2019, *ApJS*, 245, 13, doi: [10.3847/1538-4365/ab4a7e](https://doi.org/10.3847/1538-4365/ab4a7e)

Bouma, L. G., Palumbo, E. K., & Hillenbrand, L. A. 2023, *ApJL*, 947, L3, doi: [10.3847/2041-8213/acc589](https://doi.org/10.3847/2041-8213/acc589)

Boyle, A. W., Mann, A. W., & Bush, J. 2025, *ApJ*, 985, 233, doi: [10.3847/1538-4357/adcecc](https://doi.org/10.3847/1538-4357/adcecc)

Brasseur, C. E., Phillip, C., Fleming, S. W., Mullally, S. E., & White, R. L. 2019,, Astrophysics Source Code Library, record ascl:1905.007 <http://ascl.net/1905.007>

Campello, R. J. G. B., Moulavi, D., & Sander, J. 2013, in Advances in Knowledge Discovery and Data Mining, ed. J. Pei, V. S. Tseng, L. Cao, H. Motoda, & G. Xu (Berlin, Heidelberg: Springer Berlin Heidelberg), 160–172

Cantat-Gaudin, T., Jordi, C., Vallenari, A., et al. 2018, *A&A*, 618, A93, doi: [10.1051/0004-6361/201833476](https://doi.org/10.1051/0004-6361/201833476)

Claytor, Z. R., van Saders, J. L., Cao, L., et al. 2024, *ApJ*, 962, 47, doi: [10.3847/1538-4357/ad159a](https://doi.org/10.3847/1538-4357/ad159a)

Clementini, G., Ripepi, V., Garofalo, A., et al. 2023, *A&A*, 674, A18, doi: [10.1051/0004-6361/202243964](https://doi.org/10.1051/0004-6361/202243964)

Colman, I. L., Angus, R., David, T., et al. 2024, *AJ*, 167, 189, doi: [10.3847/1538-3881/ad2c86](https://doi.org/10.3847/1538-3881/ad2c86)

Colman, I. L., Huber, D., Bedding, T. R., et al. 2017, *MNRAS*, 469, 3802, doi: [10.1093/mnras/stx1056](https://doi.org/10.1093/mnras/stx1056)

Covey, K. R., Agüeros, M. A., Law, N. M., et al. 2016, *Astrophysical Journal*, 822, 81, doi: [10.3847/0004-637X/822/2/81](https://doi.org/10.3847/0004-637X/822/2/81)

Cummings, J. D., & Kalirai, J. S. 2018, *AJ*, 156, 165, doi: [10.3847/1538-3881/aad5df](https://doi.org/10.3847/1538-3881/aad5df)

Curtis, J. L., Agüeros, M. A., Mamajek, E. E., Wright, J. T., & Cummings, J. D. 2019, *AJ*, 158, 77, doi: [10.3847/1538-3881/ab2899](https://doi.org/10.3847/1538-3881/ab2899)

Douglas, S. T., Curtis, J. L., Agüeros, M. A., et al. 2019, *ApJ*, 879, 100, doi: [10.3847/1538-4357/ab2468](https://doi.org/10.3847/1538-4357/ab2468)

Eyer, L., Audard, M., Holl, B., et al. 2023, *A&A*, 674, A13, doi: [10.1051/0004-6361/202244242](https://doi.org/10.1051/0004-6361/202244242)

Feinstein, A. D., Montet, B. T., Foreman-Mackey, D., et al. 2019, *PASP*, 131, 094502, doi: [10.1088/1538-3873/ab291c](https://doi.org/10.1088/1538-3873/ab291c)

Fernandez, J. A., & Salgado, C. W. 1980, *A&AS*, 39, 11

Frasca, A., Alonso-Santiago, J., Catanzaro, G., & Bragaglia, A. 2023, *MNRAS*, 522, 4894, doi: [10.1093/mnras/stad1310](https://doi.org/10.1093/mnras/stad1310)

Fritzewski, D. J., Barnes, S. A., James, D. J., & Strassmeier, K. G. 2021a, *A&A*, 652, A60, doi: [10.1051/0004-6361/202140894](https://doi.org/10.1051/0004-6361/202140894)

Fritzewski, D. J., Barnes, S. A., James, D. J., Järvinen, S. P., & Strassmeier, K. G. 2021b, *A&A*, 656, A103, doi: [10.1051/0004-6361/202140896](https://doi.org/10.1051/0004-6361/202140896)

Fritzewski, D. J., Barnes, S. A., James, D. J., et al. 2019, *A&A*, 622, A110, doi: [10.1051/0004-6361/201833587](https://doi.org/10.1051/0004-6361/201833587)

Gaia Collaboration, Babusiaux, C., van Leeuwen, F., et al. 2018, *A&A*, 616, A10, doi: [10.1051/0004-6361/201832843](https://doi.org/10.1051/0004-6361/201832843)

Gaia Collaboration, Vallenari, A., Brown, A. G. A., et al. 2023, *A&A*, 674, A1, doi: [10.1051/0004-6361/202243940](https://doi.org/10.1051/0004-6361/202243940)

Ginsburg, A., Sipőcz, B. M., Brasseur, C. E., et al. 2019, *AJ*, 157, 98, doi: [10.3847/1538-3881/aafc33](https://doi.org/10.3847/1538-3881/aafc33)

Han, T., & Brandt, T. D. 2023, *AJ*, 165, 71, doi: [10.3847/1538-3881/acaaa7](https://doi.org/10.3847/1538-3881/acaaa7)

Harris, C. R., Millman, K. J., van der Walt, S. J., et al. 2020, *Nature*, 585, 357–362, doi: [10.1038/s41586-020-2649-2](https://doi.org/10.1038/s41586-020-2649-2)

Hattori, S., Angus, R., Foreman-Mackey, D., Lu, Y. L., & Colman, I. 2025, *AJ*, 170, 15, doi: [10.3847/1538-3881/add0ab](https://doi.org/10.3847/1538-3881/add0ab)

Hattori, S., Foreman-Mackey, D., Hogg, D. W., et al. 2022, *AJ*, 163, 284, doi: [10.3847/1538-3881/ac625a](https://doi.org/10.3847/1538-3881/ac625a)

Herschel, John Frederick William, S. 1847, *Results of astronomical observations made during the years 1834, 5, 6, 7, 8, at the Cape of Good Hope; being the completion of a telescopic survey of the whole surface of the visible heavens, commenced in 1825*

Higgins, M. E., & Bell, K. J. 2023, *AJ*, 165, 141, doi: [10.3847/1538-3881/acb20c](https://doi.org/10.3847/1538-3881/acb20c)

Howell, S. B., Sobeck, C., Haas, M., et al. 2014, *Publications of the Astronomical Society of the Pacific*, 126, 398, doi: [10.1086/676406](https://doi.org/10.1086/676406)

Hunt, E. L., & Reffert, S. 2021, *A&A*, 646, A104, doi: [10.1051/0004-6361/202039341](https://doi.org/10.1051/0004-6361/202039341)

Hunt, E. L., & Reffert, S. 2023, *A&A*, 673, A114, doi: [10.1051/0004-6361/202346285](https://doi.org/10.1051/0004-6361/202346285)

Hunter, J. D. 2007, *Computing in Science and Engineering*, 9, 90, doi: [10.1109/MCSE.2007.55](https://doi.org/10.1109/MCSE.2007.55)

Jones, E., Oliphant, T., Peterson, P., et al. 2001, <http://www.scipy.org/>

Koelbloed, D. 1959, *BAN*, 14, 265

Kounkel, M., & Covey, K. 2019, *AJ*, 158, 122, doi: [10.3847/1538-3881/ab339a](https://doi.org/10.3847/1538-3881/ab339a)

Kounkel, M., Covey, K., & Stassun, K. G. 2020, *AJ*, 160, 279, doi: [10.3847/1538-3881/abc0e6](https://doi.org/10.3847/1538-3881/abc0e6)

Lightkurve Collaboration, Cardoso, J. V. d. M., Hedges, C., et al. 2018, *Astrophysics Source Code Library* <http://ascl.net/1812.013>

Lomb, N. R. 1976, *Ap&SS*, 39, 447, doi: [10.1007/BF00648343](https://doi.org/10.1007/BF00648343)

McInnes, L., Healy, J., & Astels, S. 2017, *The Journal of Open Source Software*, 2, 205, doi: [10.21105/joss.00205](https://doi.org/10.21105/joss.00205)

Mowlavi, N., Holl, B., Lecoeur-Taïbi, I., et al. 2023, *A&A*, 674, A16, doi: [10.1051/0004-6361/202245330](https://doi.org/10.1051/0004-6361/202245330)

Nardiello, D., Borsato, L., Piotto, G., et al. 2019, *MNRAS*, 490, 3806, doi: [10.1093/mnras/stz2878](https://doi.org/10.1093/mnras/stz2878)

Newton, E. R., Rampalli, R., Kraus, A. L., et al. 2022, *AJ*, 164, 115, doi: [10.3847/1538-3881/ac8154](https://doi.org/10.3847/1538-3881/ac8154)

Ochsenbein, F., Bauer, P., & Marcout, J. 2000, *A&AS*, 143, 23, doi: [10.1051/aas:2000169](https://doi.org/10.1051/aas:2000169)

Oelkers, R. J., & Stassun, K. G. 2018, *AJ*, 156, 132, doi: [10.3847/1538-3881/aad68e](https://doi.org/10.3847/1538-3881/aad68e)

Pass, E. K., Charbonneau, D., Irwin, J. M., & Winters, J. G. 2022, *ApJ*, 936, 109, doi: [10.3847/1538-4357/ac7da8](https://doi.org/10.3847/1538-4357/ac7da8)

Petrucci, R. P., Gómez Maqueo Chew, Y., Jofré, E., Segura, A., & Ferrero, L. V. 2024, *MNRAS*, 527, 8290, doi: [10.1093/mnras/stad3720](https://doi.org/10.1093/mnras/stad3720)

Popinchalk, M., Faherty, J. K., Curtis, J. L., et al. 2023, *ApJ*, 945, 114, doi: [10.3847/1538-4357/acb055](https://doi.org/10.3847/1538-4357/acb055)

Press, W. H., & Rybicki, G. B. 1989, *Astrophysical Journal*, 338, 277, doi: [10.1086/167197](https://doi.org/10.1086/167197)

Rampalli, R., Agüeros, M. A., Curtis, J. L., et al. 2021, *ApJ*, 921, 167, doi: [10.3847/1538-4357/ac0c1e](https://doi.org/10.3847/1538-4357/ac0c1e)

Rebull, L. M., Stauffer, J. R., Hillenbrand, L. A., et al. 2022, *AJ*, 164, 80, doi: [10.3847/1538-3881/ac75f1](https://doi.org/10.3847/1538-3881/ac75f1)

Rebull, L. M., Stauffer, J. R., Bouvier, J., et al. 2016, *AJ*, 152, 113, doi: [10.3847/0004-6256/152/5/113](https://doi.org/10.3847/0004-6256/152/5/113)

Ricker, G. R., Winn, J. N., Vanderspek, R., et al. 2015, *J. Astron. Telesc. Instrum. Syst.*, 1, 014003, doi: [10.1117/1.JATIS.1.1.014003](https://doi.org/10.1117/1.JATIS.1.1.014003)

Ripepi, V., Clementini, G., Molinaro, R., et al. 2023, *A&A*, 674, A17, doi: [10.1051/0004-6361/202243990](https://doi.org/10.1051/0004-6361/202243990)

Roelens, M., Eyer, L., Mowlavi, N., et al. 2018, *A&A*, 620, A197, doi: [10.1051/0004-6361/201833357](https://doi.org/10.1051/0004-6361/201833357)

Scargle, J. D. 1982, *ApJ*, 263, 835, doi: [10.1086/160554](https://doi.org/10.1086/160554)

STScI. 2022, *STScI/MAST*, doi: [10.17909/0CP4-2J79](https://doi.org/10.17909/0CP4-2J79)

The Astropy Collaboration, Price-Whelan, A. M., Sipócz, B. M., et al. 2018, *ArXiv e-prints* <https://arxiv.org/abs/1801.02634>

Van-Lane, P. R., Speagle, J. S., Eadie, G. M., et al. 2025, *ApJ*, 986, 59, doi: [10.3847/1538-4357/adc73](https://doi.org/10.3847/1538-4357/adc73)

Wang, D., Hogg, D. W., Foreman-Mackey, D., & Schölkopf, B. 2016, *PASP*, 128, 094503, doi: [10.1088/1538-3873/128/967/094503](https://doi.org/10.1088/1538-3873/128/967/094503)

Wenger, M., Ochsenbein, F., Egret, D., et al. 2000, *A&AS*, 143, 9, doi: [10.1051/aas:2000332](https://doi.org/10.1051/aas:2000332)